XIV School on Synchrotron Radiation:
Fundamentals, Methods and Applications
Muggia, Italy / 18-29 September 2017

SILS
SOCIETA' ITALIANA DI LUCE DI SINCROTRONE

Elettra Sincrotrone Trieste

Diffraction from nanocrystalline materials

Paolo.Scardi@unitn.it

Special thanks to: Mirco D'Incau, Camilo Perez Demydenko, Alberto Flor & Luca Rebuffi

PRESENTATION OUTLINE

PART I

Diffraction from nanocrystalline materials: reciprocal space vs direct space methods

PART II

A case study: highly deformed nanocrystalline metals

PART III

Total Scattering methods

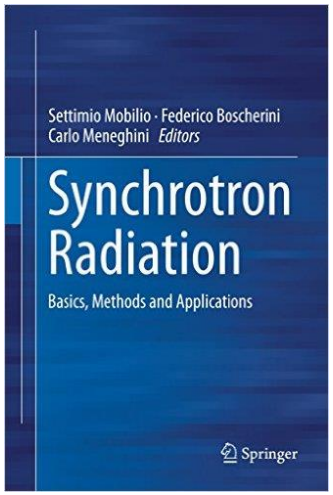

Chapter VIII
X-ray diffraction by crystalline materials
Davide Viterbo e Giuseppe Zanotti

Chapter X
Powder diffraction and synchrotron radiation
Gilberto Artioli

→ **Chapter XVIII**
Diffraction from nanocrystalline materials
Paolo Scardi

→ **Talk (today at 12:00 h)**
Powder diffraction and synchrotron radiation
J.R. Plaisier

FROM SINGLE-CRYSTAL TO POWDER DIFFRACTION

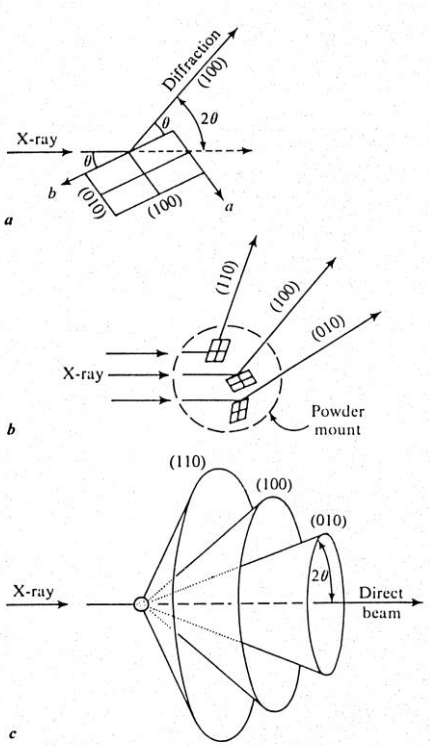

FIGURE 10.11 Diffraction of monochromatic x-rays from (a) a single crystal and (b) an aggregate of small mineral fragments. (c) Diffraction cones produced by the powder method.

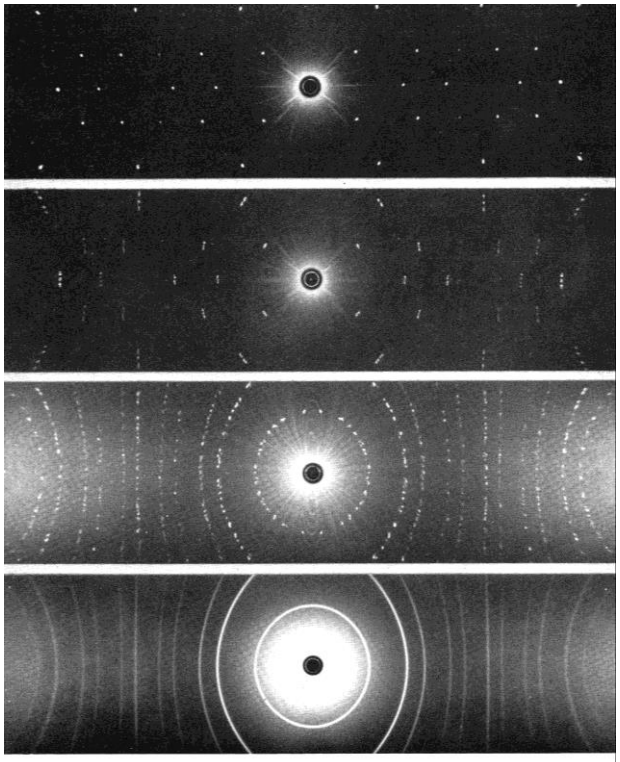

(*From top to bottom*). Fig. 197: Single-crystal rotation photograph of fluorite [100] vertical: Fig. 198; Single-crystal rotation photograph of fluorite [100] 2° to vertical: Fig. 199; X-ray photograph of five randomly oriented crystals of fluorite: Fig. 200; Powder photograph of fluorite.

Laue diffraction conditions

$$\mathbf{a} \cdot (\mathbf{s} - \mathbf{s}_o) = h\lambda$$
$$\mathbf{b} \cdot (\mathbf{s} - \mathbf{s}_o) = k\lambda$$
$$\mathbf{c} \cdot (\mathbf{s} - \mathbf{s}_o) = l\lambda$$

Bragg's law

$$2d(hkl)\sin\theta = \lambda$$

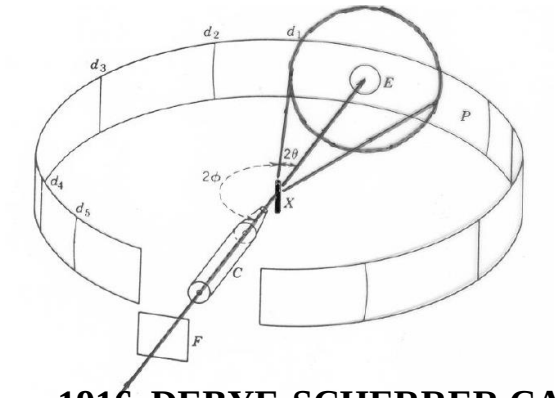

1916 DEBYE-SCHERRER CAMERA

XRD FROM SMALL CRYSTALS: SCHERRER EQUATION

Determination of the size and internal structure of colloid particles by means of x-rays

by

P. Scherrer.

Presented by P. Debye in the meeting of **26. Juli 1918.**

... ... The theory provides for the half-value width ***h*** of the maximum defined in the known manner, which occurs at the angle ϑ to the incident X-ray beam, the value:

$$h = 2\sqrt{\frac{ln\,2}{\pi}} \cdot \frac{\lambda}{\Lambda} \cdot \frac{1}{\cos\vartheta/2}.$$

λ/Λ is the ratio of the wavelength of the monochromatic X-rays used to the edge of the crystal presumed to be cube-shaped

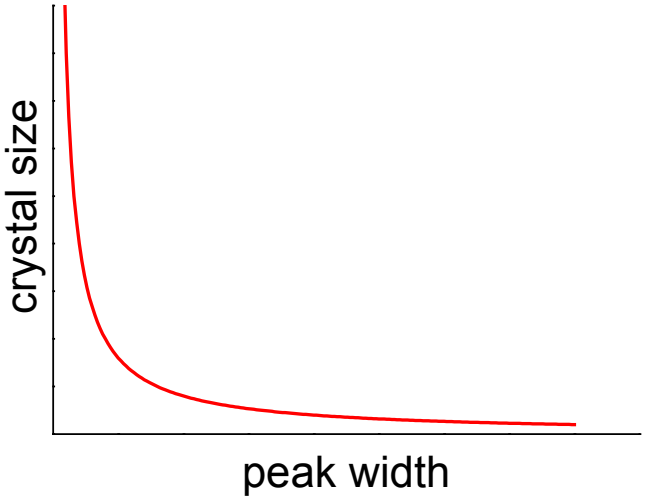

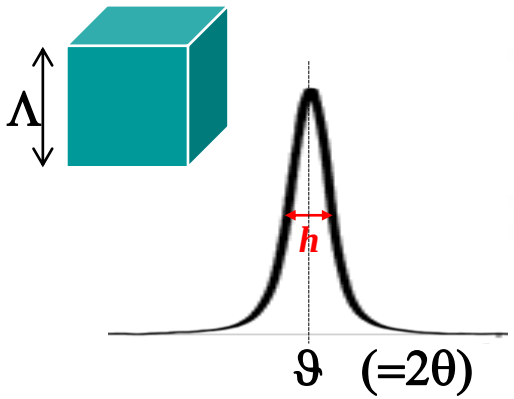

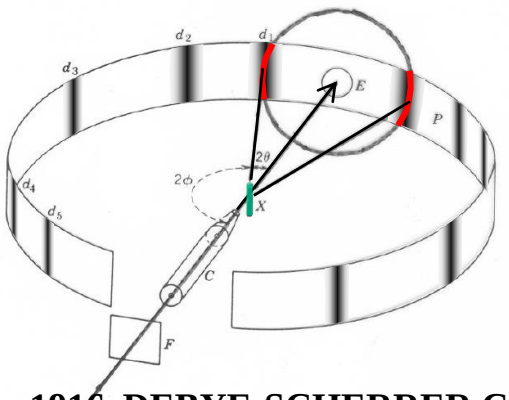

1916 DEBYE-SCHERRER CAMERA

LABORATORY vs SYNCHROTRON RADIATION XRD

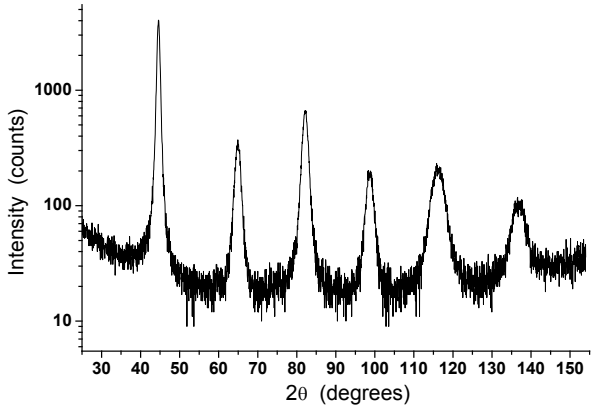

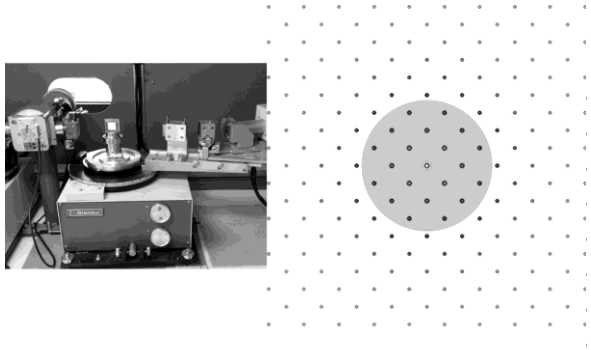

Powder diffraction data from a ball milled Fe1.5%Mo powder collected on a traditional laboratory instrument (Rigaku PMG-VH, Bragg-Brentano geometry) with CuKα radiation (λ=0.1540598 nm). On the right: schematic of reciprocal space with extension of the limiting sphere (radius 2/λ).

Fig. 1 in P. Scardi & L. Gelisio, Chapter XVIII, "Diffraction from nanocrystalline materials"

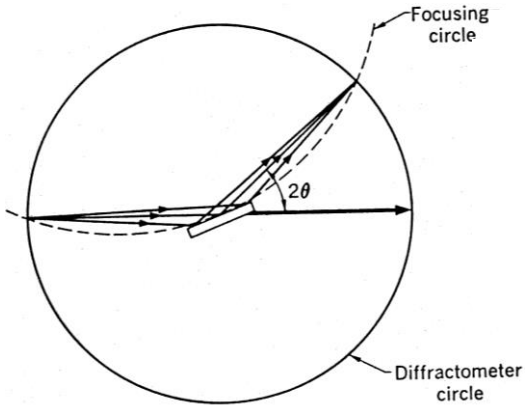

Powder diffractometer geometry

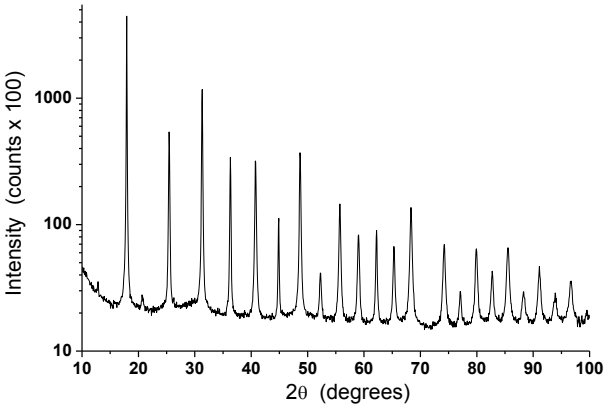

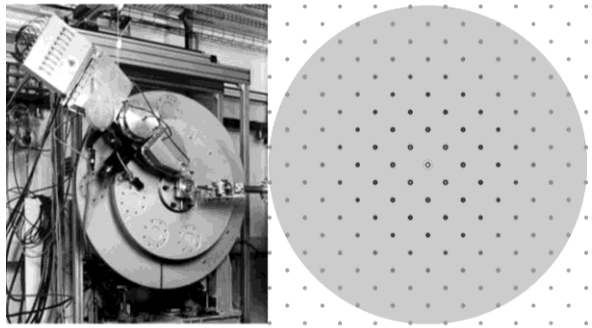

Powder diffraction data from a ball milled Fe1.5%Mo powder collected (b) on ID31 (now ID22) at ESRF, Grenoble (F) (λ=0.0632 nm). On the right: schematic of reciprocal space with extension of the limiting sphere (radius 2/λ).

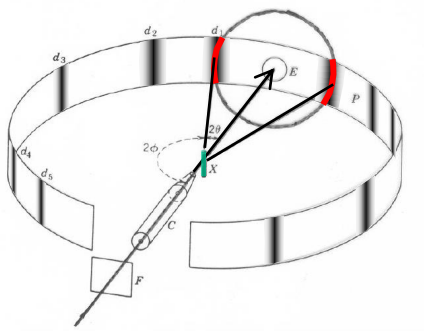

1916 Debye-Scherrer geometry
(the return !)

Powder diffraction and synchrotron radiation
J.R. Plaisier (today at 12:00 h)

DIFFRACTION PATTERN FROM A POLYCRYSTALLINE

powder
(bulk polycrystalline)

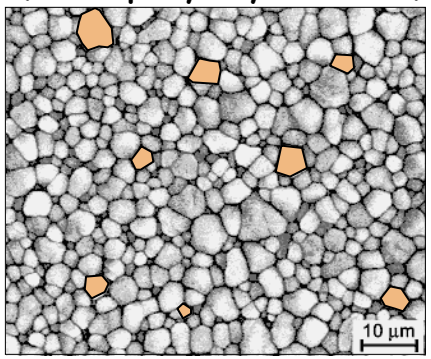

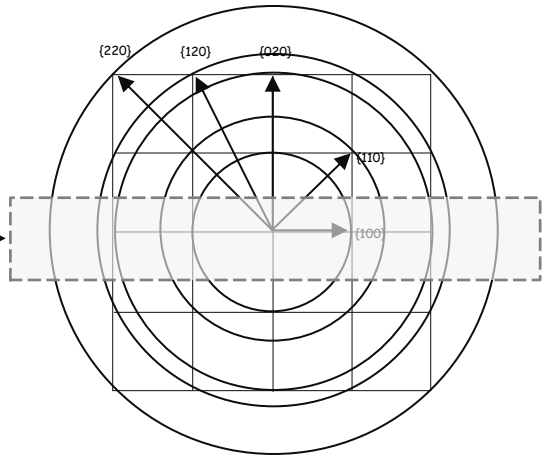

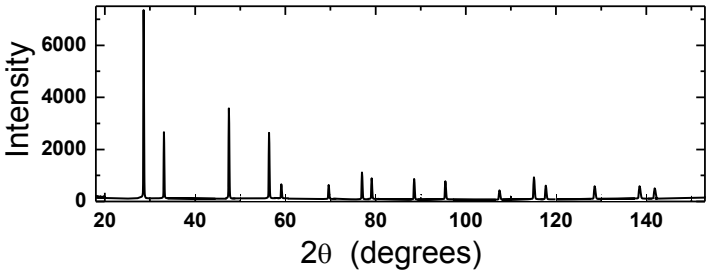

nanocrystalline
powder

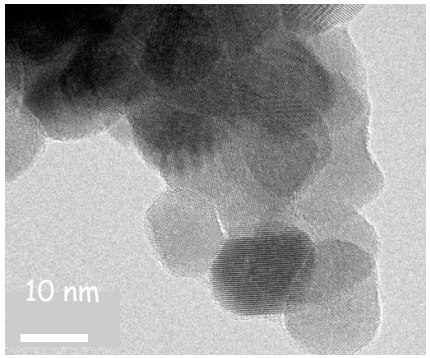

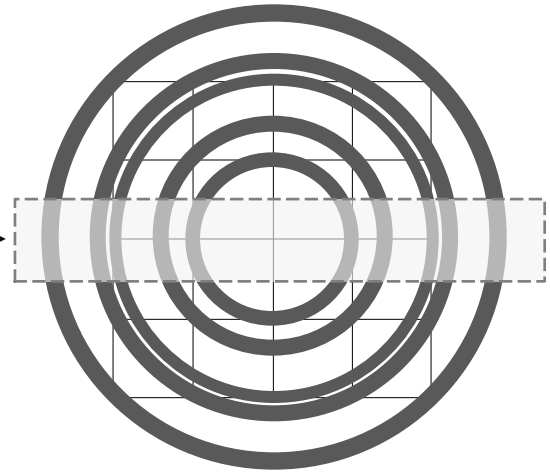

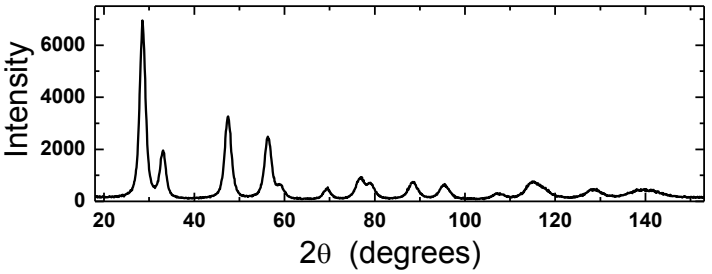

DIFFRACTION FROM NANOCRYSTALLINE *POWDER*

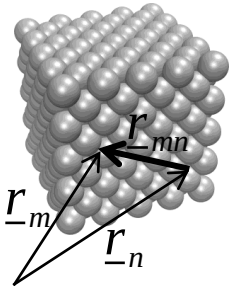

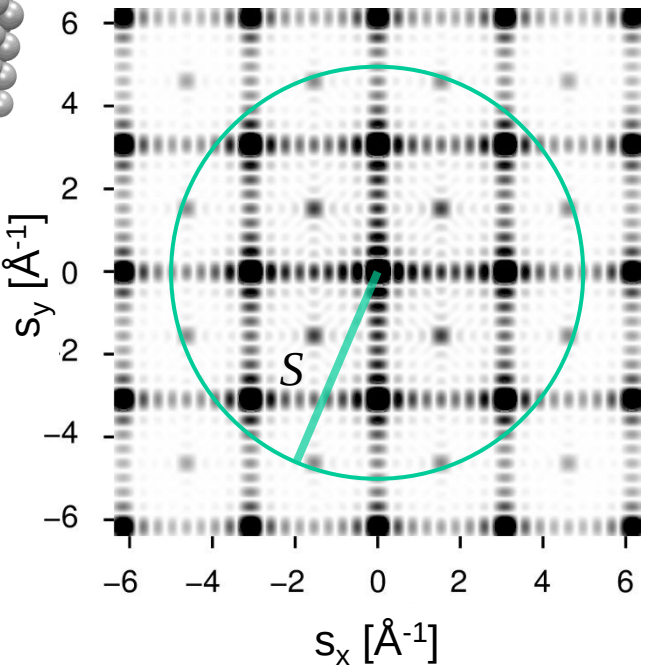

orientational (or powder) average

$$I_{PD}(s) \propto \frac{\int I_{sc}(s,\vartheta,\phi)\,d\Omega}{4\pi s^2}$$

$s=Q/2\pi=2\sin\theta/\lambda$

$$d\Omega = s^2 \sin\vartheta\, d\vartheta\, d\phi$$

$$I_{sc}(\underline{s}) \propto \sum_m f_m e^{2\pi i(\underline{s}\cdot\underline{r}_m)} \sum_n f_n^* e^{-2\pi i(\underline{s}\cdot\underline{r}_n)} = \sum_m \sum_n f_m f_n^* e^{2\pi i(\underline{s}\cdot\underline{r}_{mn})}$$

DIFFRACTION FROM NANOCRYSTALLINE *POWDER*

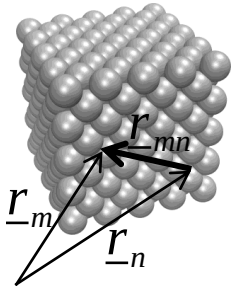

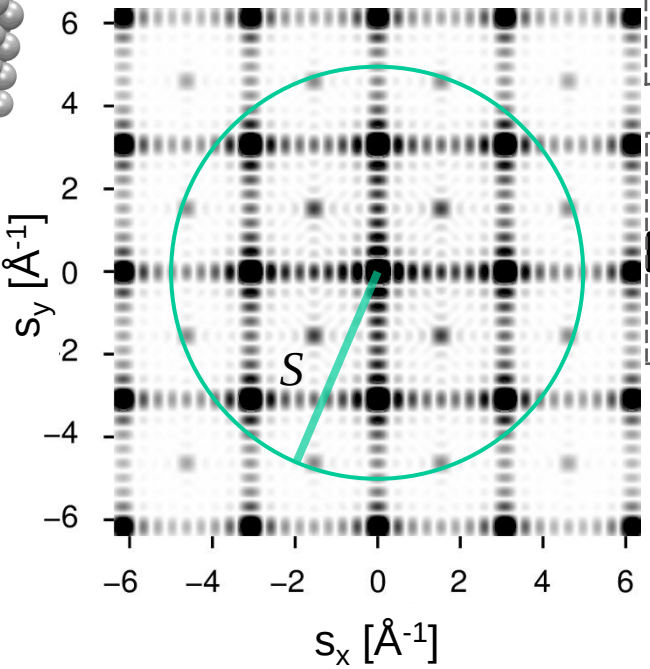

Traditional "reciprocal space" approach

(1) sum, then average

or

(2) average, then sum

Debye scattering equation, "direct space"

Total scattering approach

$$I_{PD}(s) \propto \frac{\int \sum_m \sum_n f_m f_n^* e^{2\pi i(\underline{s}\cdot\underline{r}_{mn})} d\Omega}{4\pi s^2}$$

$s=Q/2\pi=2\sin\theta/\lambda$

$$d\Omega = s^2 \sin\vartheta d\vartheta d\phi$$

$$I_{sc}(\underline{s}) \propto \sum_m f_m e^{2\pi i(\underline{s}\cdot\underline{r}_m)} \sum_n f_n^* e^{-2\pi i(\underline{s}\cdot\underline{r}_n)} = \sum_m \sum_n f_m f_n^* e^{2\pi i(\underline{s}\cdot\underline{r}_{mn})}$$

DIFFRACTION FROM NANOCRYSTALLINE *POWDER*

Traditional "reciprocal space" approach (sum, then average)

1. Factorize the contribution of a unit cell
   ($|F|^2$ – F, structure factor)

$$D = Na$$

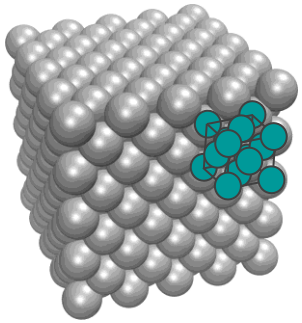

2. Build the diffraction signal as interference between unit cells

$$I_{sc} \propto |F|^2 \sum_{h'=-\infty}^{\infty} \sum_{k'=-\infty}^{\infty} \sum_{l'=-\infty}^{\infty} \frac{\sin^2(\pi N h)}{\pi^2 (h-h')^2} \frac{\sin^2(\pi N k)}{\pi^2 (k-k')^2} \frac{\sin^2(\pi N l)}{\pi^2 (l-l')^2}$$

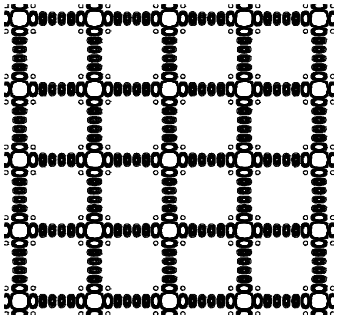

3. Integrate over the powder diffraction sphere (orientational average)

$$I_{PD}(s) \propto \frac{\int I_{sc}(\underline{s}) d\Omega}{4\pi s^2}$$

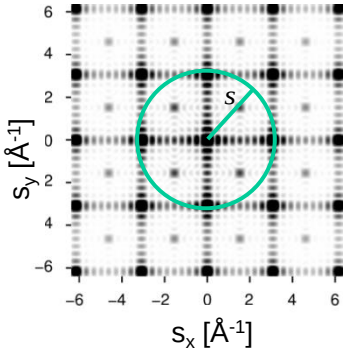

$$\boxed{I(s) \propto |F|^2 \Phi(s, D)}$$

line profile function

DIFFRACTION FROM NANOCRYSTALLINE *POWDER*

Fourier Transform of peak profile: the Common Volume Function

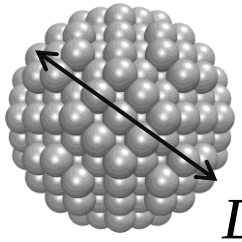

$D = 100$ Å

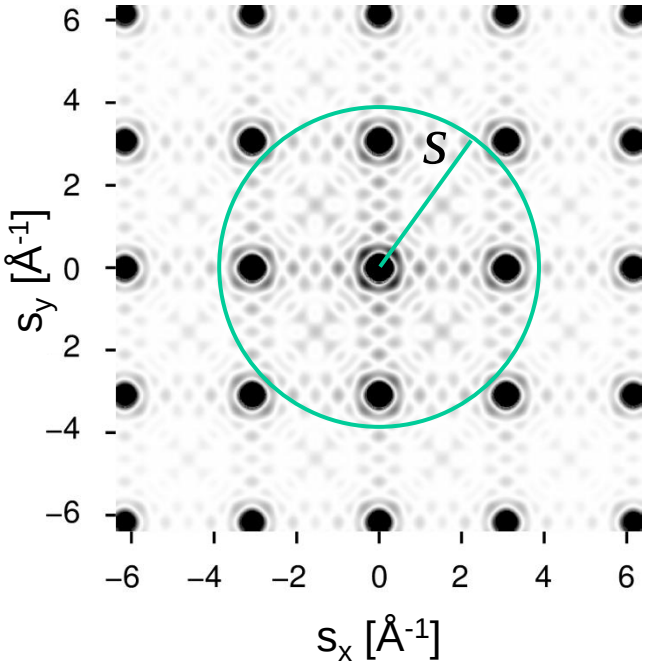

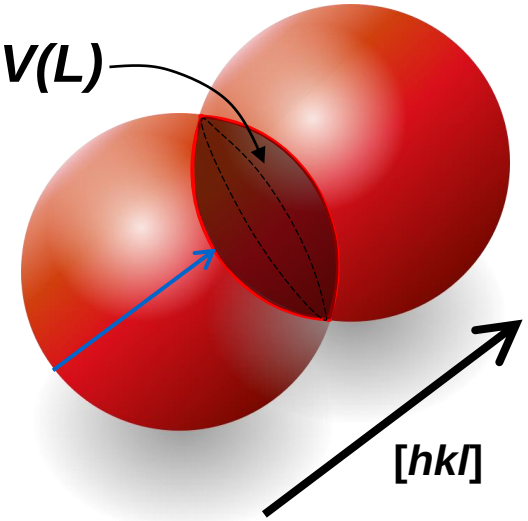

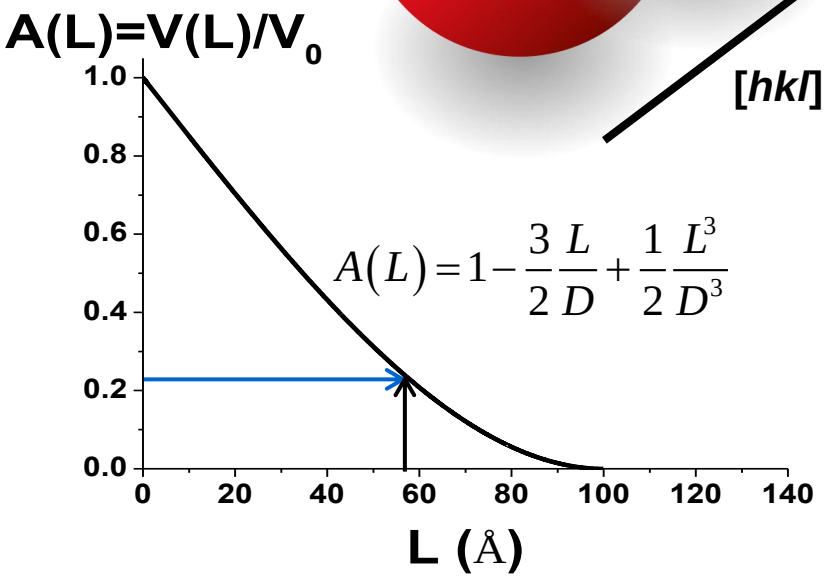

$$I_{PD}(s) \propto |F|^2 \Phi_{sphere}(s,D) = |F|^2 \int_0^D A(L)\cos(2\pi sL)\,dL$$

DIFFRACTION FROM NANOCRYSTALLINE *POWDER*

Fourier Transform of peak profile: the Common Volume Function

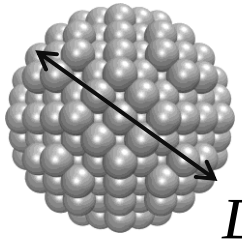

$D = 100$ Å

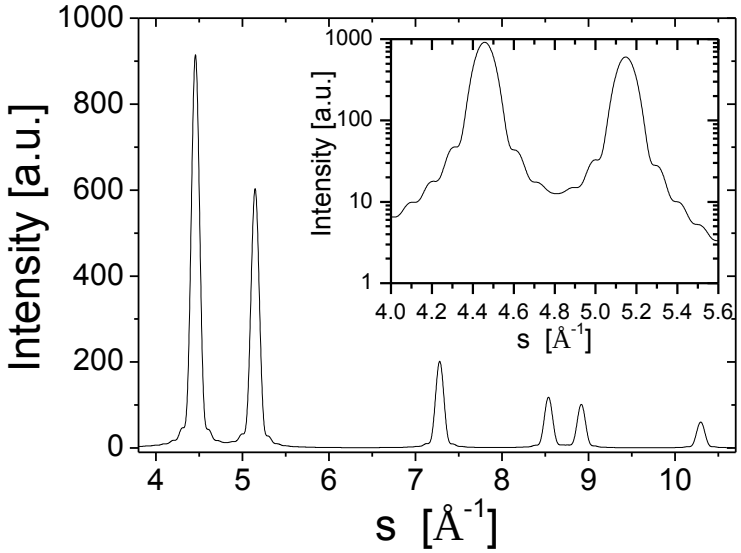

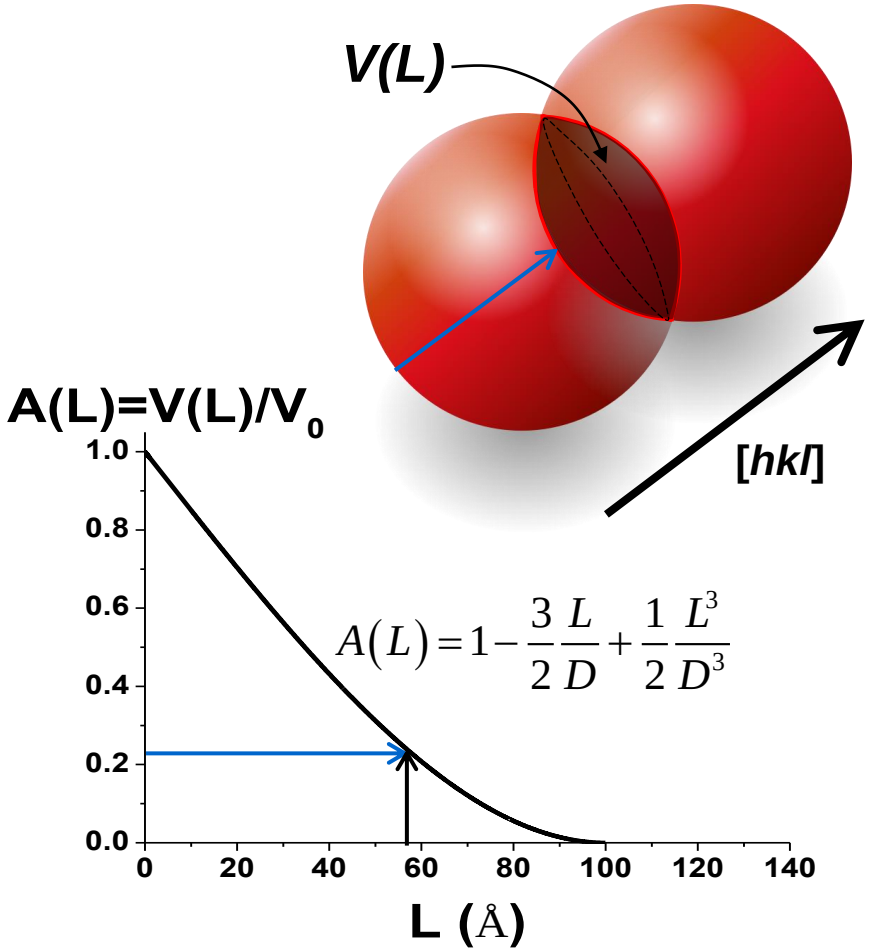

$$I_{PD}(s) \propto |F|^2 \Phi_{sphere}(s,D) = |F|^2 \int_0^D A(L)\cos(2\pi sL)\,dL$$

DIFFRACTION FROM NANOCRYSTALLINE *POWDER*

ESRF – ID31 (now ID22)
λ=0.0632 nm

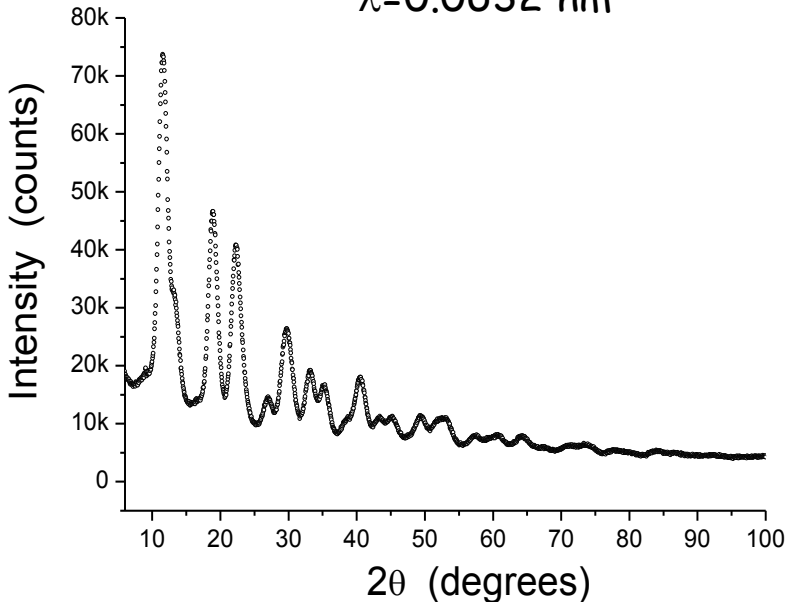

Xerogel cerium oxide powder

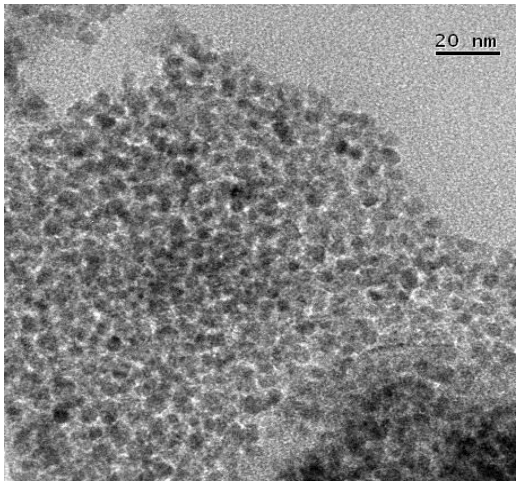

$$A_{sphere}(L) = 1 - \frac{3}{2}\frac{L}{D} + \frac{1}{2}\frac{L^3}{D^3}$$

$$A_{\ln,sphere}(L) = \sum_{n=0}^{3} H_n \operatorname{erfc}\left[\frac{\ln|L| - \mu - (3-n)\sigma^2}{\sigma\sqrt{2}}\right] \exp\left\{-\frac{n}{2}\left[2\mu + (6-n)\sigma^2\right]\right\} |L|^n$$

H_0=½, H_1=-¾, H_2=0, H_3=¼

$$g(D) = \frac{1}{D\sigma(2\pi)^{1/2}} e^{-(\ln D - \mu)^2/2\sigma^2}$$

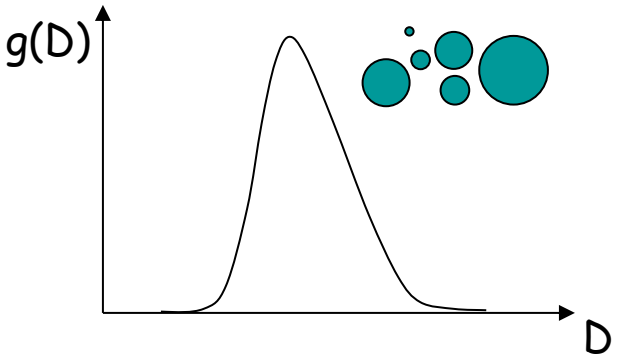

polydisperse system

Scardi, P. (2008). Powder Diffraction: Theory and Practice, edited by R. E. Dinnebier & S. J. L. Billinge, ch. 13, pp. 376–413. Cambridge: Royal Society of Chemistry

DIFFRACTION FROM NANOCRYSTALLINE *POWDER*

ESRF – ID31 (now ID22)

λ=0.0632 nm

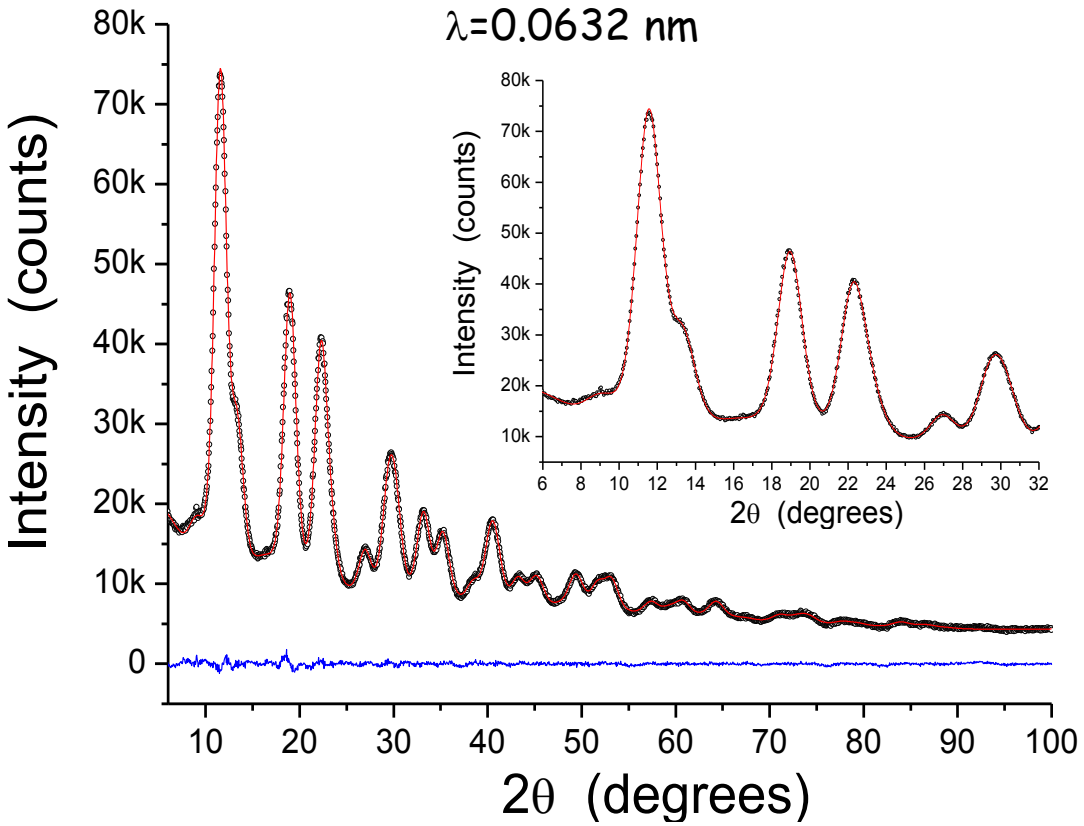

Xerogel cerium oxide powder

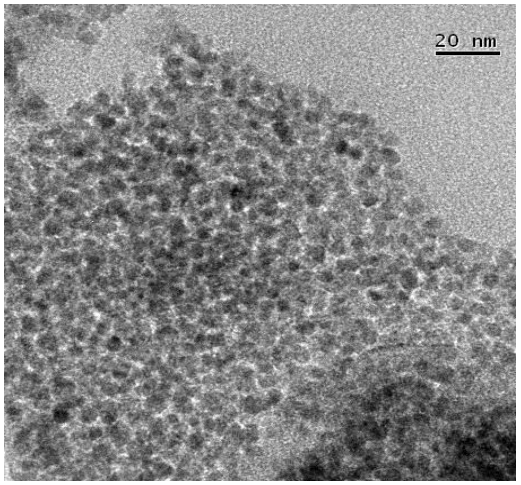

$$g(D) = \frac{1}{D\sigma(2\pi)^{1/2}} e^{-(\ln D-\mu)^2/2\sigma^2}$$

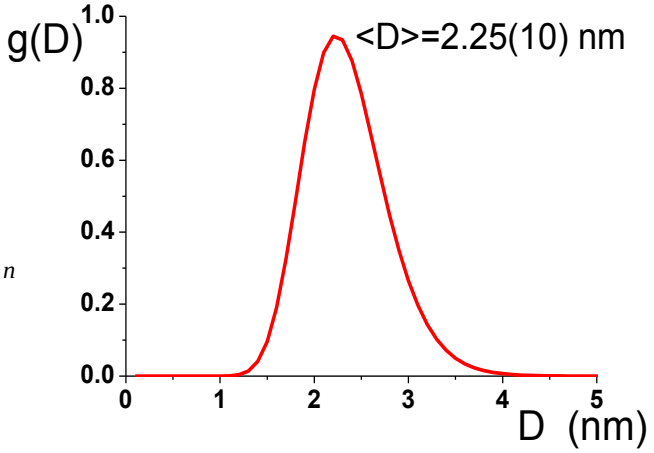

$$A_{\ln-sphere}(L) = \sum_{n=0}^{3} H_n \operatorname{erfc}\left[\frac{\ln|L| - \mu - (3-n)\sigma^2}{\sigma\sqrt{2}}\right] \exp\left\{-\frac{n}{2}\left[2\mu + (6-n)\sigma^2\right]\right\} |L|^n$$

H_0=½, H_1=-¾, H_2=0, H_3=¼

Scardi, P. (2008). Powder Diffraction: Theory and Practice, edited by R. E. Dinnebier & S. J. L. Billinge, ch. 13, pp. 376–413. Cambridge: Royal Society of Chemistry

DIFFRACTION FROM NANOCRYSTALLINE *POWDER*

Fourier Transform of peak profile: the Common Volume Function

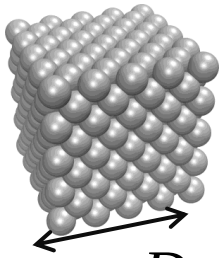

$D = 80.6$ Å

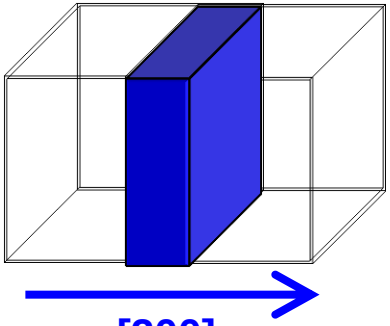

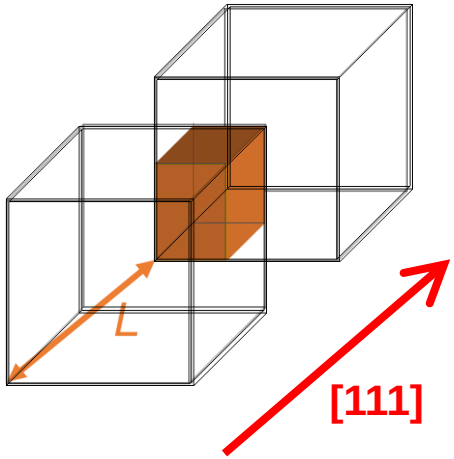

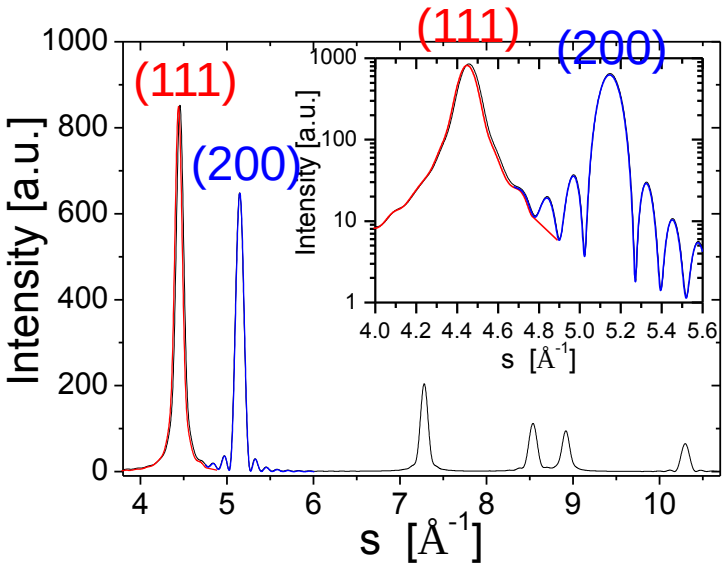

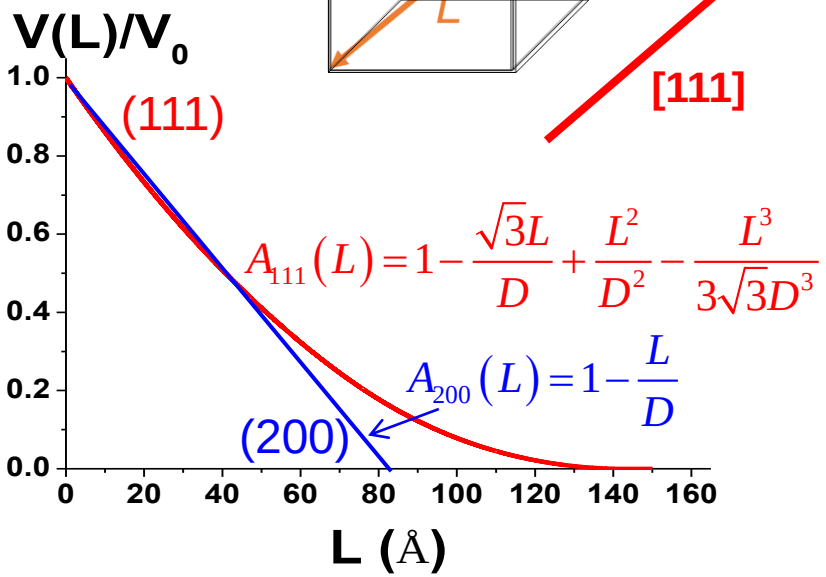

$$I_{PD}(s) \propto |F|^2 \Phi_{cube}(s,D) = |F|^2 \int_0^{L_{max}} A(L)\cos(2\pi sL)\,dL$$

DIFFRACTION FROM NANOCRYSTALLINE *POWDER*

Any shape → A.Leonardi et al., J.Appl.Cryst. 45 (2012) 1162

Wulff polyhedra

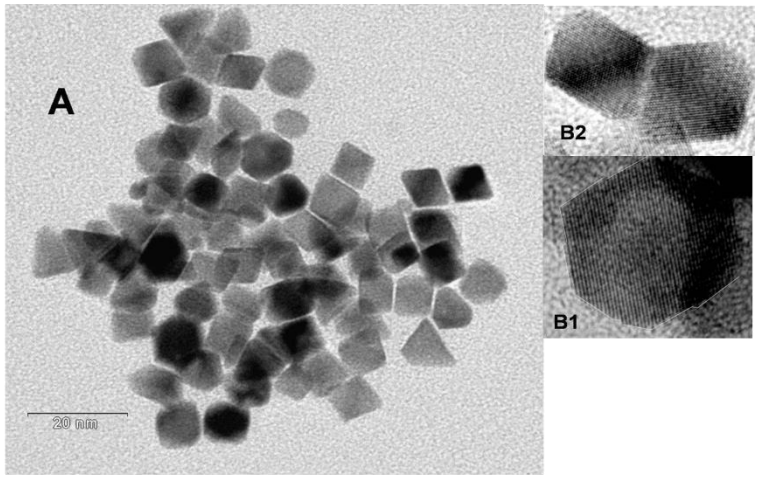

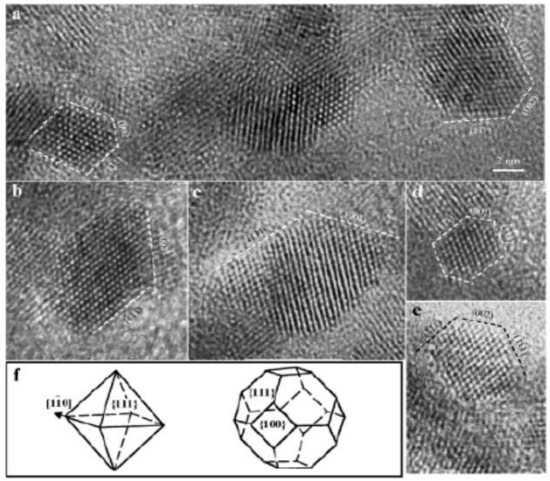

Figure 2. (a–e) Typical high-resolution TEM images of CeO_2 nanoparticles oriented along [110], showing the facet structures as defined by the {002} and {111} facets. (f) Structural models of the octahedral and truncated octahedral shapes.

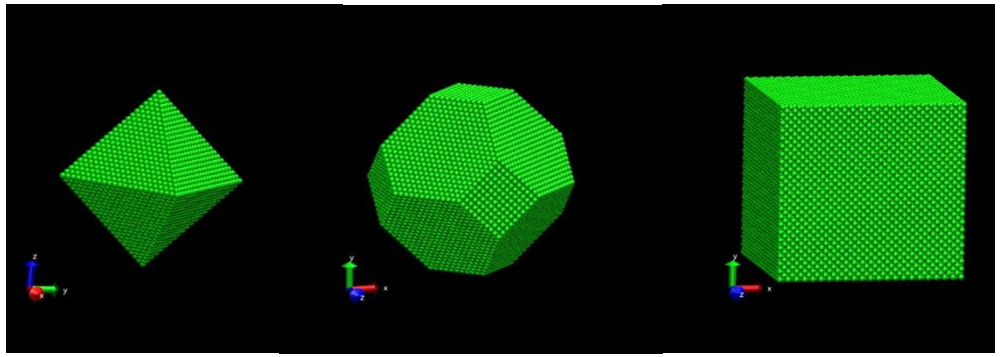

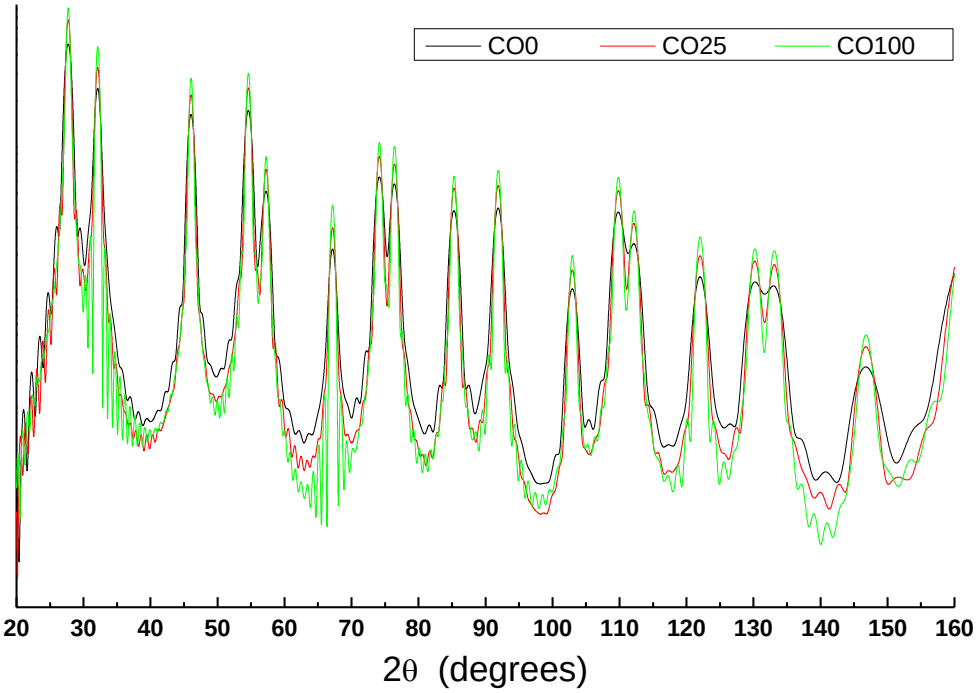

DIFFRACTION FROM NANOCRYSTALLINE *POWDER*

Pd nanocrystals

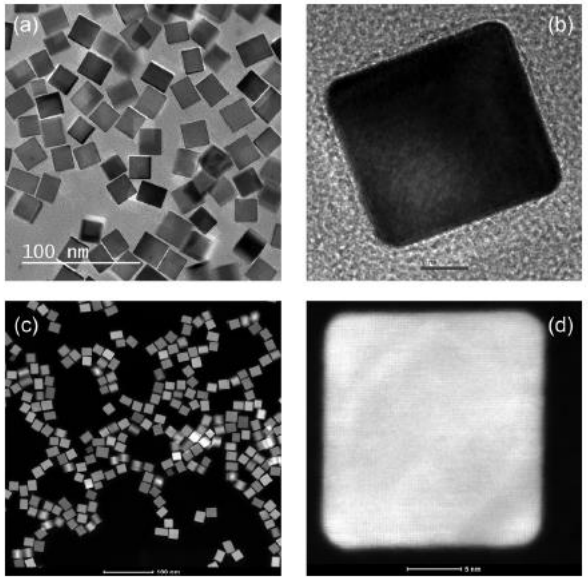

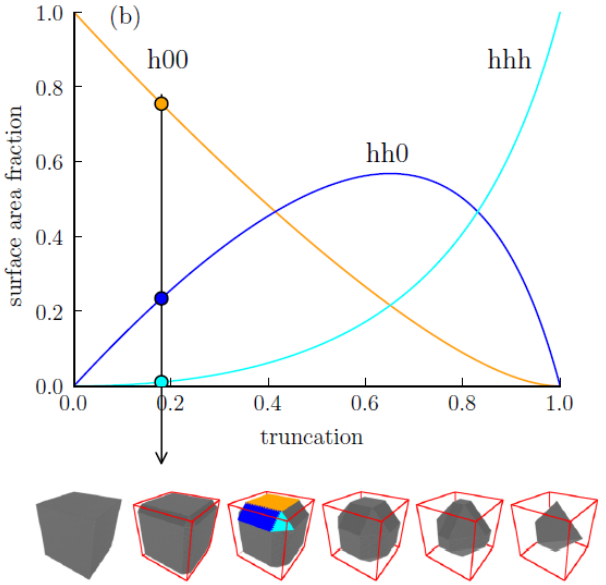

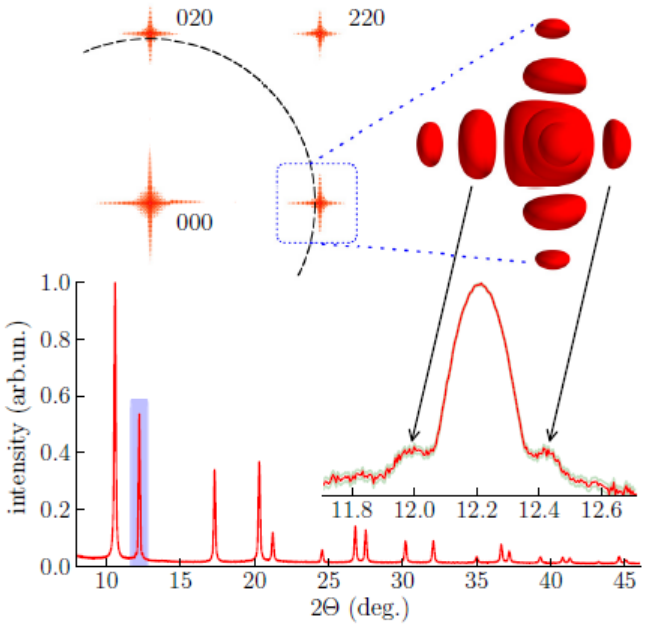

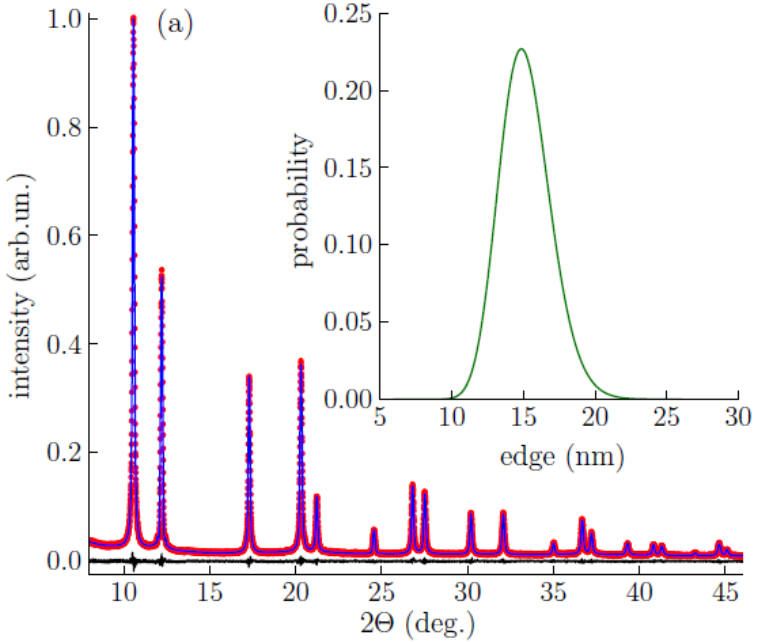

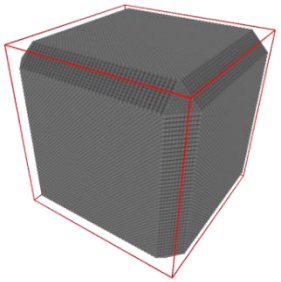

P. Scardi et al.
Phys.Rev.B 91(2015)155414

DIFFRACTION FROM NANOCRYSTALLINE *POWDER*

Any shape→ A.Leonardi et al., J.Appl.Cryst. 45 (2012) 1162

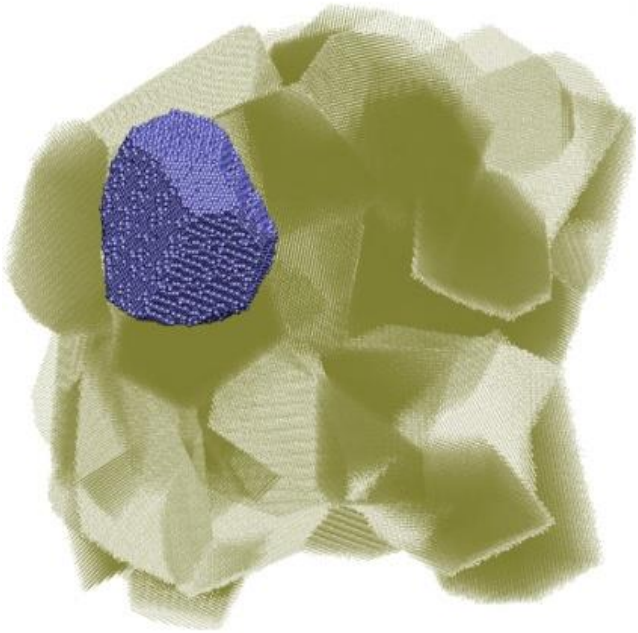

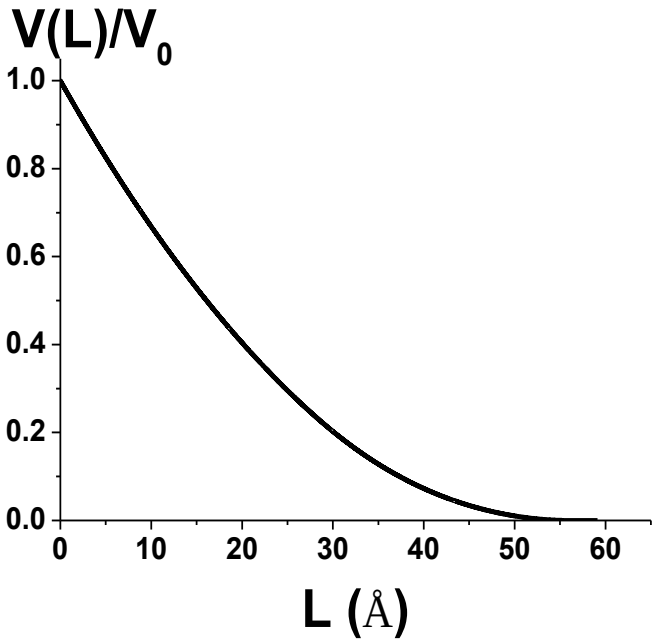

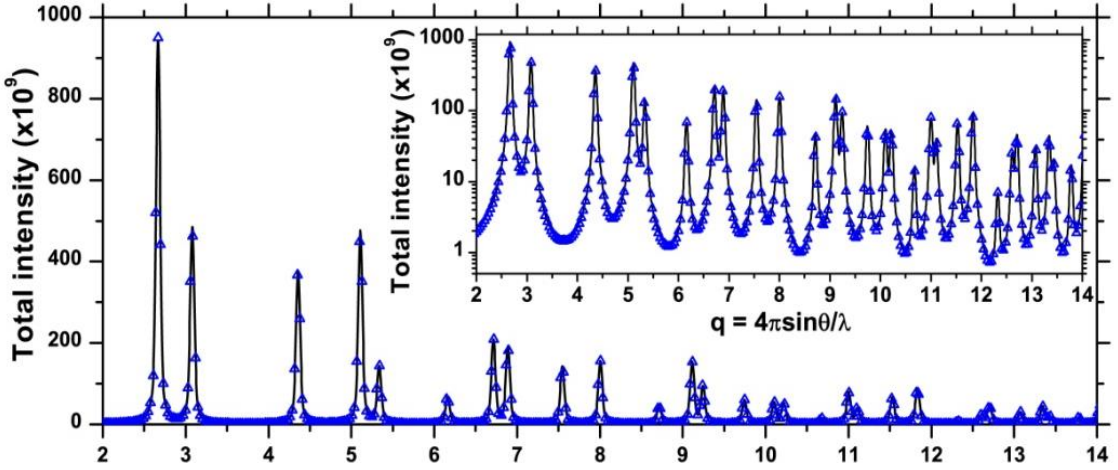

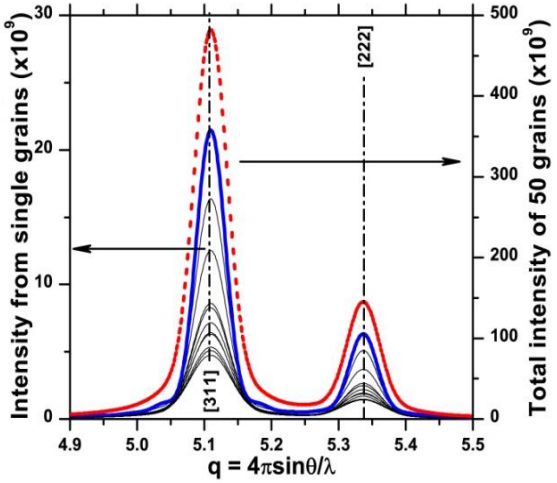

DIFFRACTION FROM NANOCRYSTALLINE *POWDER*

… what I did not consider (so far…): ***microstructure***

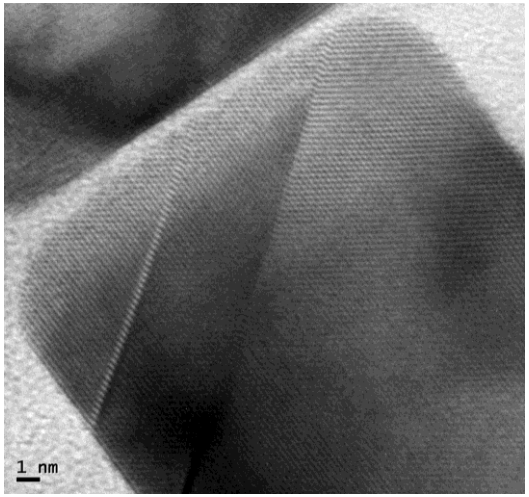

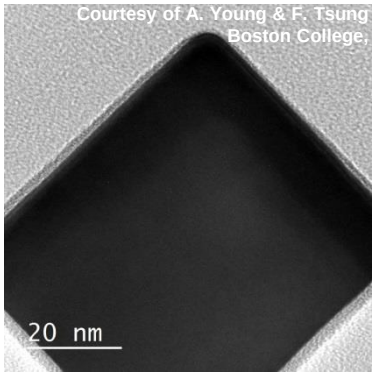

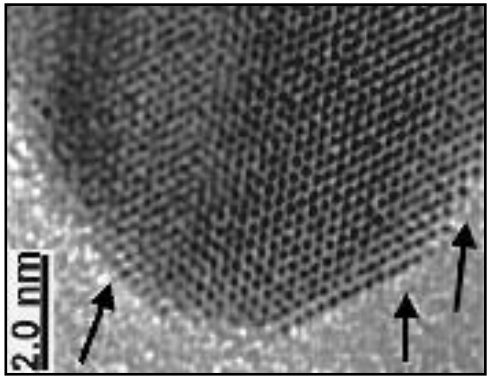

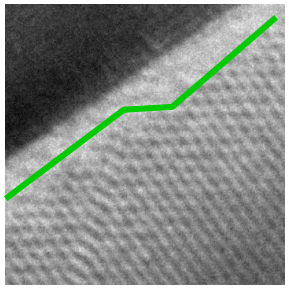

most metals:

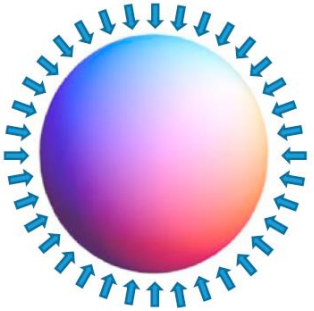

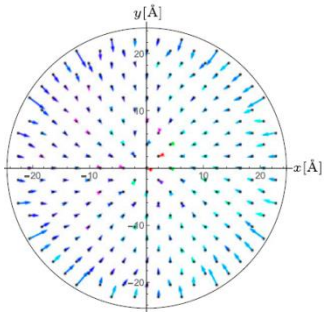

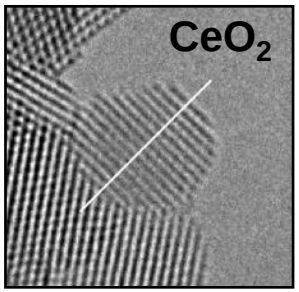

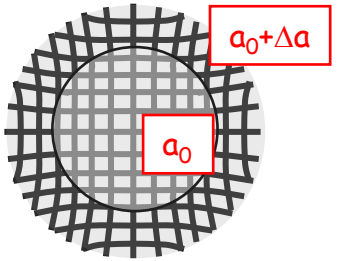

Surface relaxation
Perez-Demydenko & Scardi, Phil. Mag. 97 (2017) 2317

DIFFRACTION FROM NANOCRYSTALLINE *POWDER*

… what I did not consider (so far…): ***microstructure***

Severe Plastic Deformation

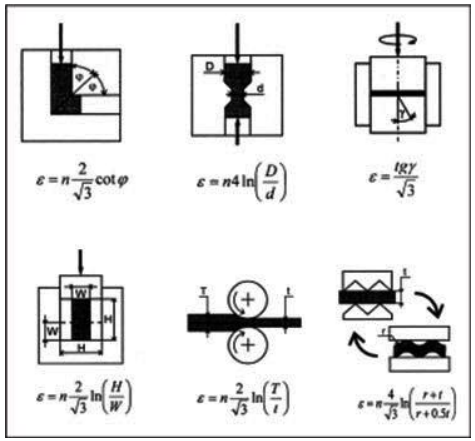

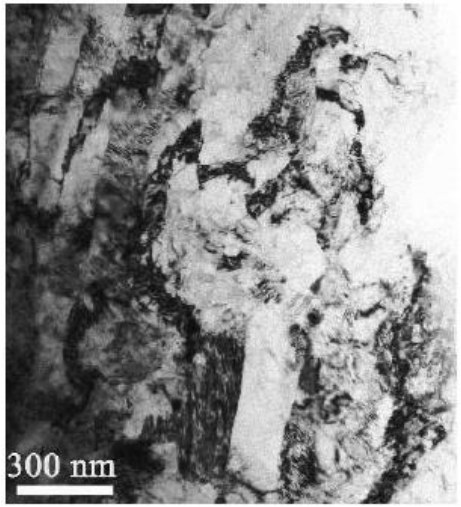

FIG. 1. Grain structures

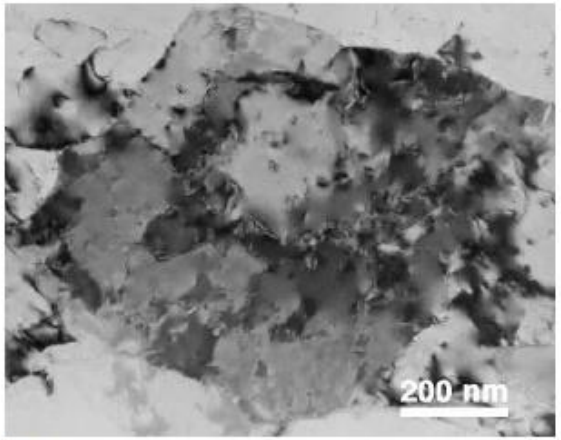

FIG. 8. Large grain containing several subgrains, which in turn contain dislocation cells.

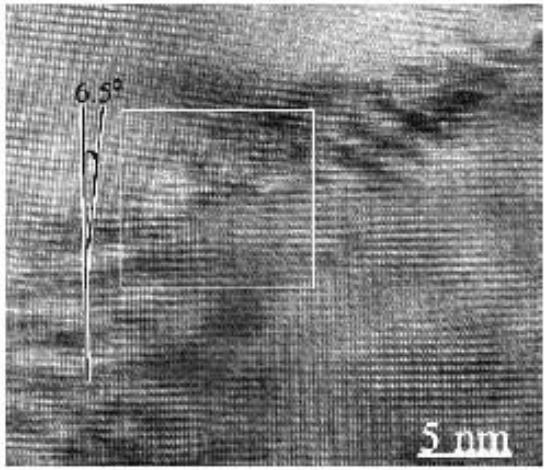

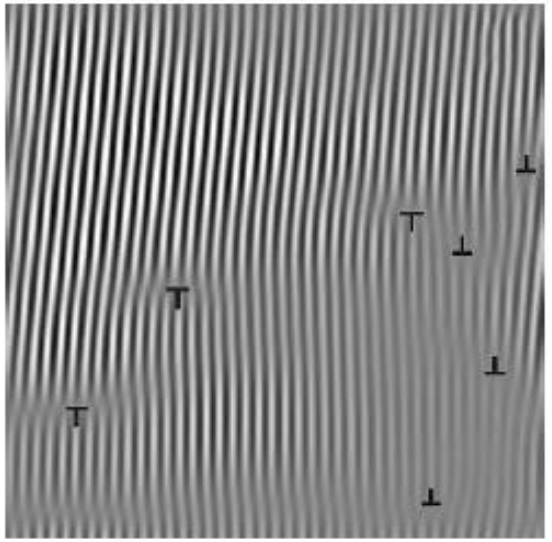

FIG. 10. (a) HRTEM image of a low-angle grain boundary with a misorientation of 6.5°, (b) Fourier-filtered image from the white frame in (a), showing the dislocation arrangement on the grain boundary

(Zhu et al. J. Mater. Res. 18 (2003) 1908)

DIFFRACTION FROM NANOCRYSTALLINE *POWDER*

microstructure → perturbation of "perfect crystal structure"

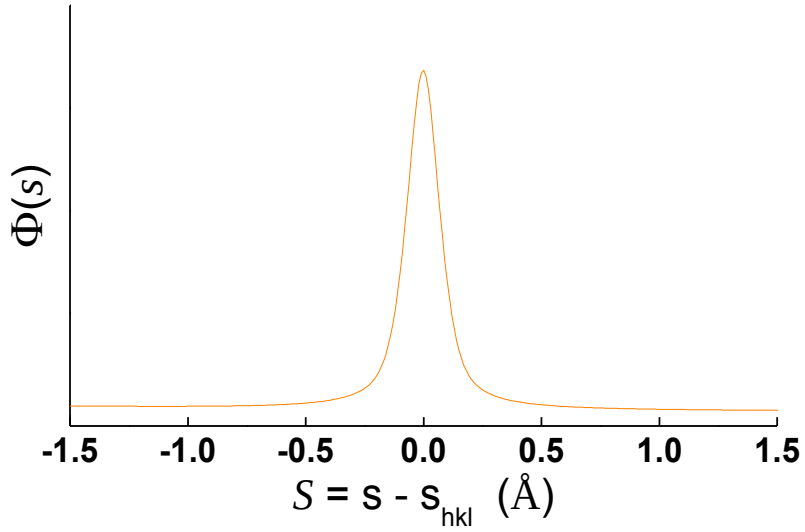

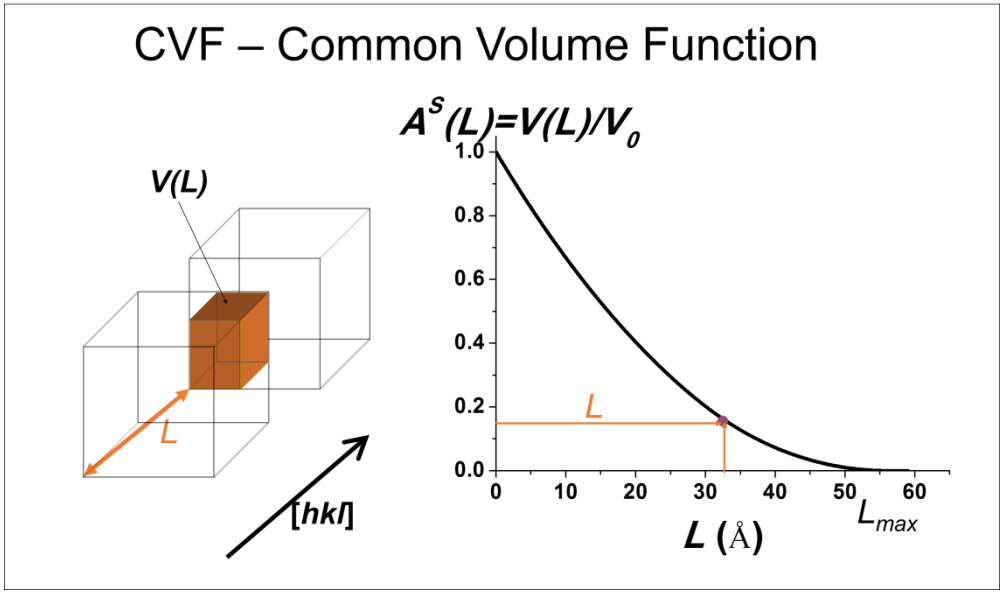

Any shape→ A.Leonardi et al., J.Appl.Cryst. 45 (2012) 1162

$$I(s) \propto |F|^2 \int_0^{L_{\max}} A^S(L)\cos(2\pi sL)\,dL$$

$$I(s) \propto \int_0^{L_{\max}} A^S(L)\left\langle FF_L^* \right\rangle e^{2\pi isL}\,dL$$

$$I(s) \propto |F|^2 \int_0^{L_{\max}} A^S\left[A^D(A^F + iB^F)\cdot\ldots\right] e^{2\pi isL}\,dL$$

domain size inhomog.strain faulting

DIFFRACTION FROM NANOCRYSTALLINE *POWDER*

Pd nanocrystals

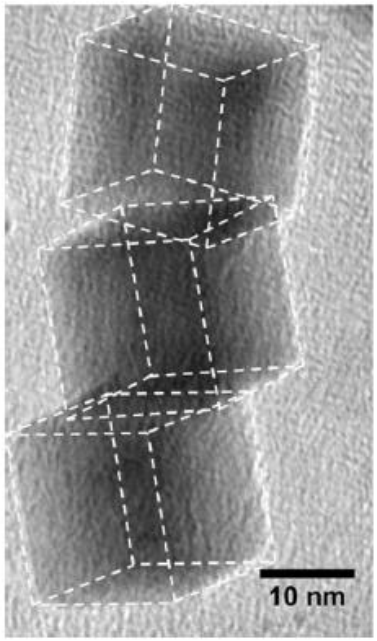

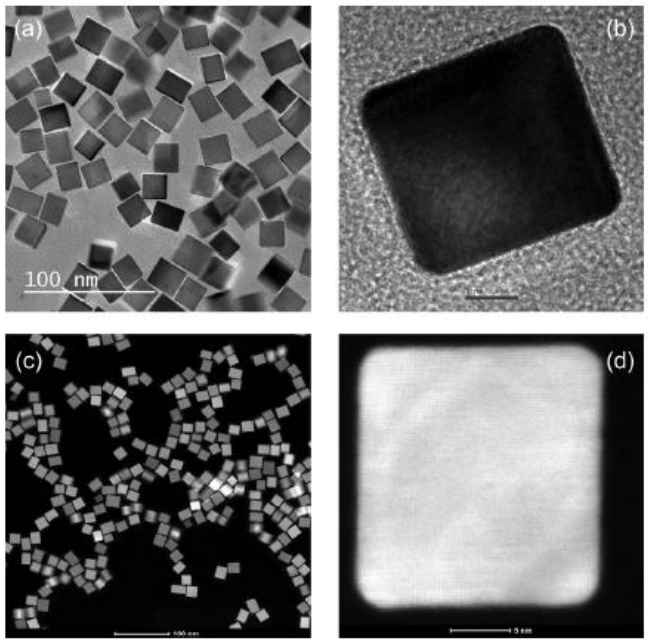

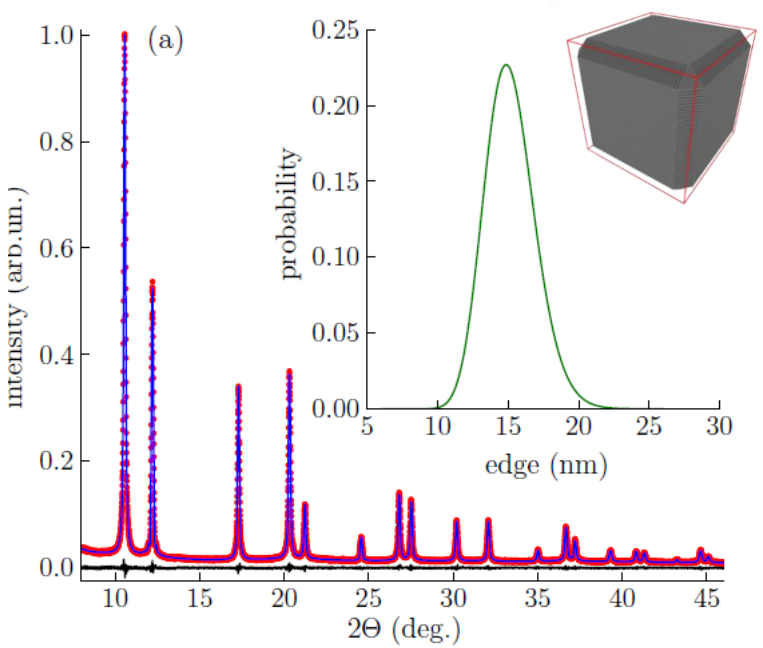

Inhomogeneous displacement
(strain, ε = ΔL/L): $A^D(L) = e^{-2\pi^2 s^2 <\Delta L_{hkl}^2>}$

$$I(s) \propto |F|^2 \int_0^{L_{max}} A^S A^D T^{IP} e^{2\pi i s L} dL$$

domain size — inhomog. strain — instrum. profile

P. Scardi et al. Phys.Rev.B 91(2015)155414

DIFFRACTION FROM NANOCRYSTALLINE *POWDER*

Displacement distribution of couples of atoms at distance *L*

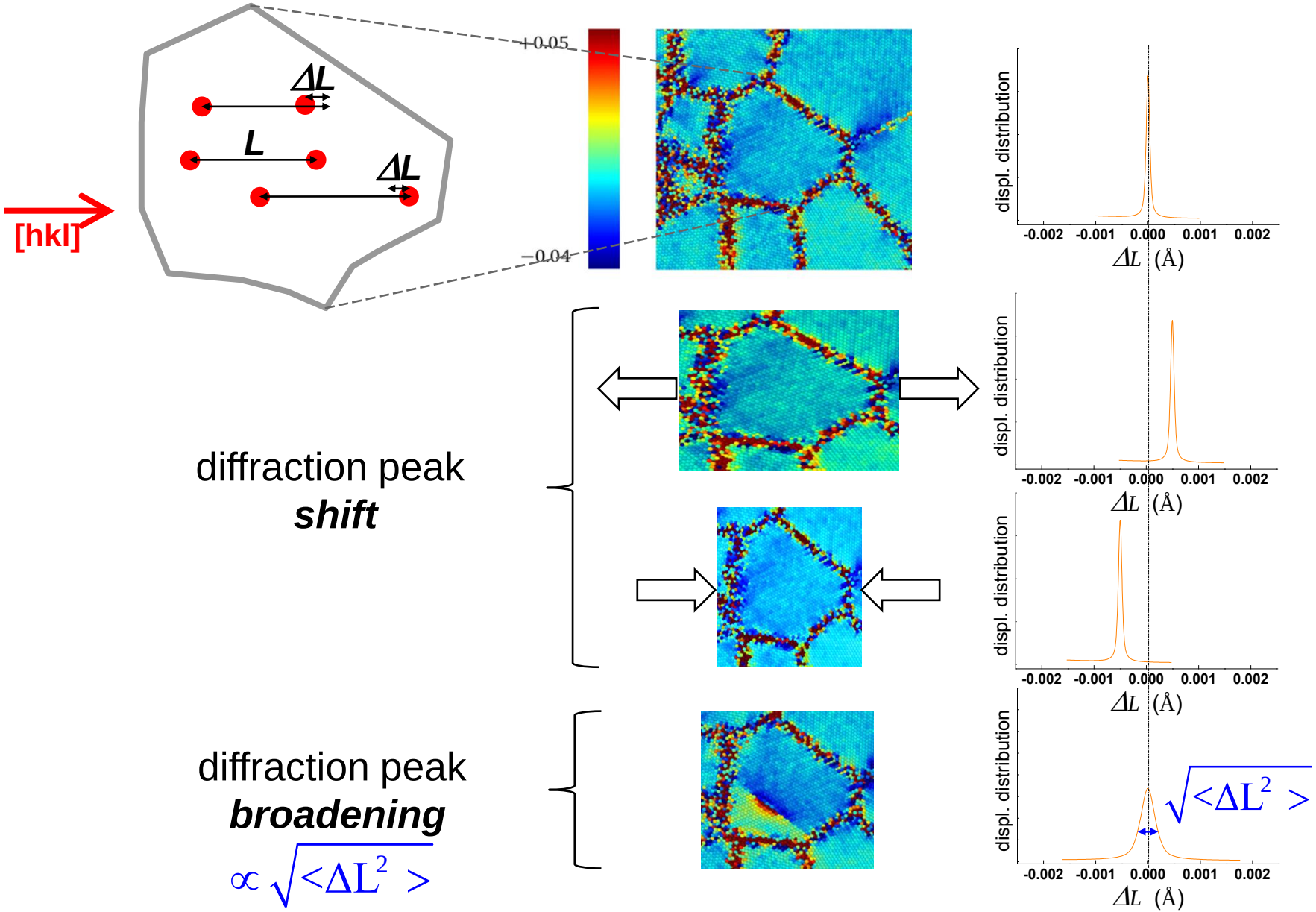

DIFFRACTION FROM NANOCRYSTALLINE *POWDER*

Pd nanocrystals

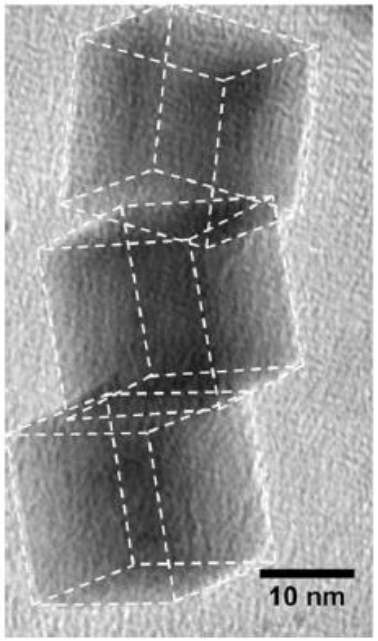

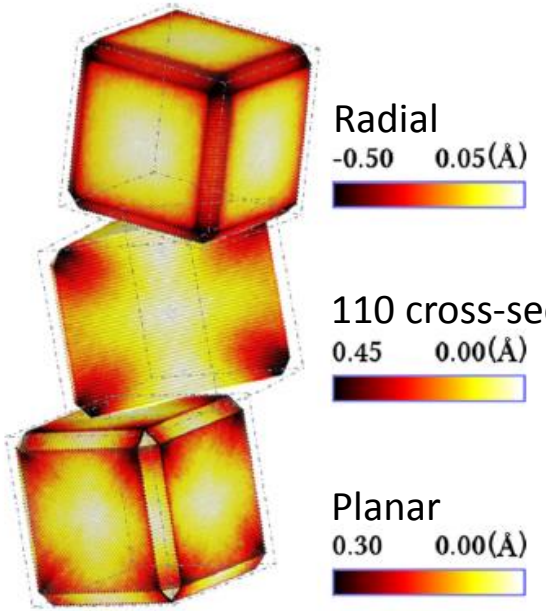

Molecular Dynamics (MD)
atomic displacement maps

Warren plot

(root mean square displacement vs L)

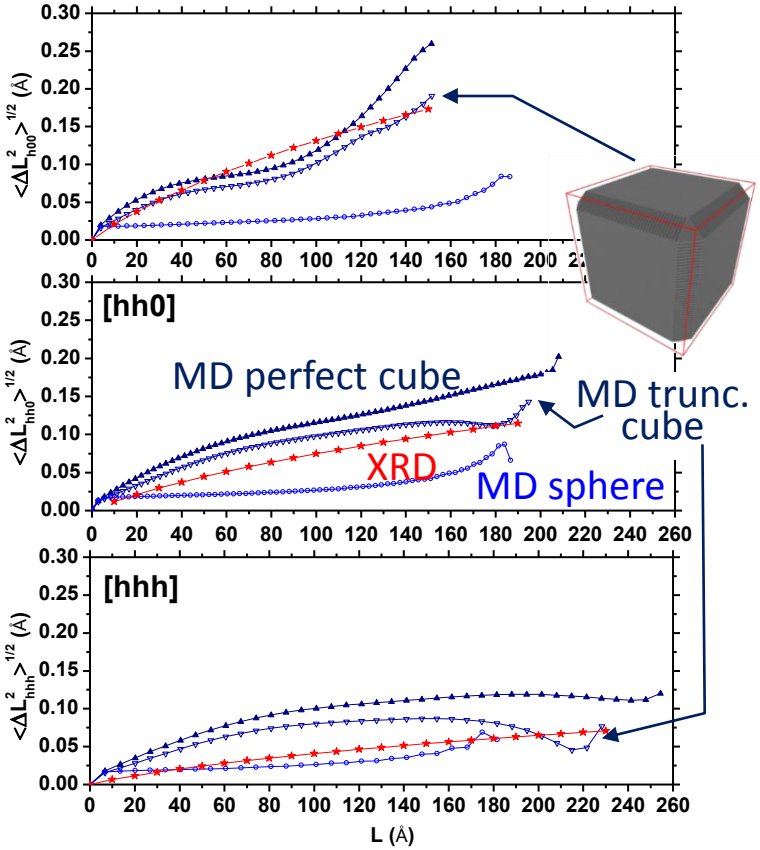

Inhomogeneous displacement
(strain, ε = ΔL/L): $A^D(L) = e^{-2\pi^2 s^2 <\Delta L_{hkl}^2>}$

$$I(s) \propto |F|^2 \int_0^{L_{max}} A^S A^D T^{IP} e^{2\pi i s L} dL$$

domain size — inhomog. strain — instrum. profile

P. Scardi et al. Phys.Rev.B 91(2015)155414

WHOLE POWDER PATTERN MODELLING – WPPM

$$I(s) \propto |F|^2 \int_0^{L_{\max}} A^S \left[A^D (A^F + iB^F) \cdot \ldots \right] T^{IP} e^{2\pi i s L} dL$$

domain size | inhomog.strain | faulting | instrum. profile

Diffraction profile as a convolution of (independent) effects:

$$I(s) = I^{IP}(s) \otimes I^S(s) \otimes I^D(s) \otimes I^F(s) \otimes I^{APB}(s) \otimes \ldots$$

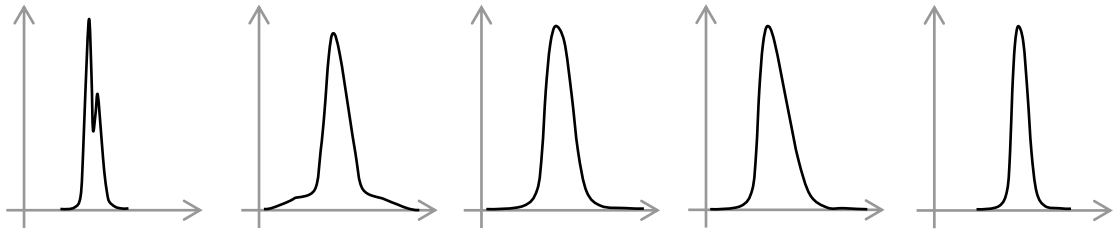

DIFFRACTION FROM NANOCRYSTALLINE *POWDER*

High-energy grinding (ball-milling) of an iron alloy powder: AstaloyTM Fe1.5Mo

SEM

TEM

HREM

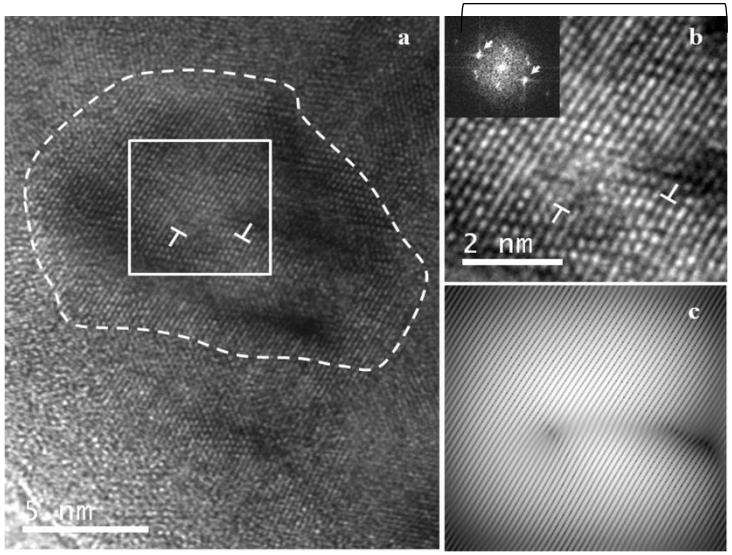

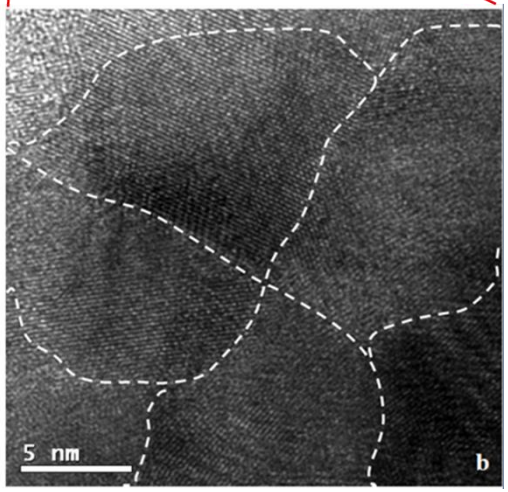

Rebuffi et al., Sci. Reports 6 (2016) 20712

DIFFRACTION FROM NANOCRYSTALLINE *POWDER*

High-energy grinding (ball-milling) of an iron alloy powder: AstaloyTM Fe1.5Mo

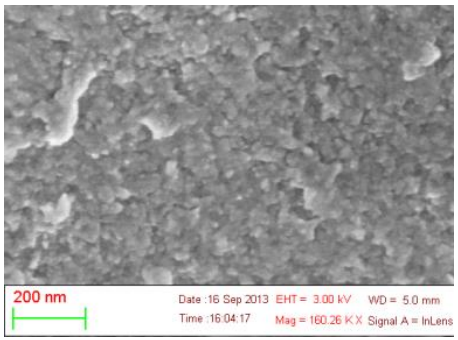

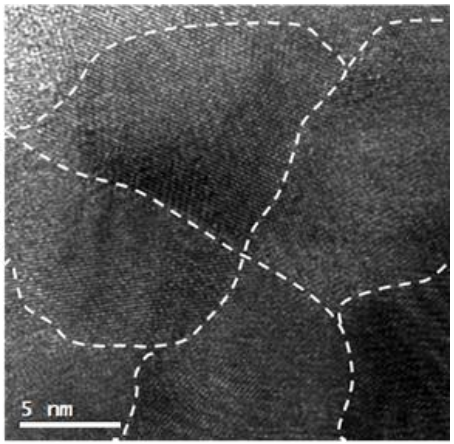

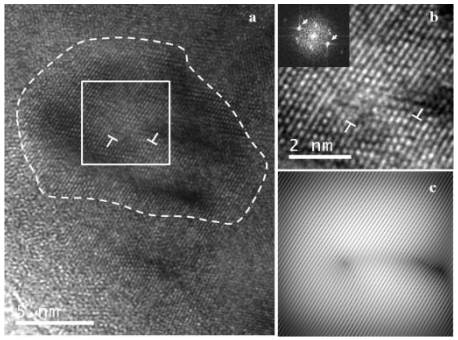

$$I_{hkl}(s) \propto |F|^2 \int A^S(L) A^D_{hkl}(L) T^{IP}(L) e^{2\pi i s L} dL$$

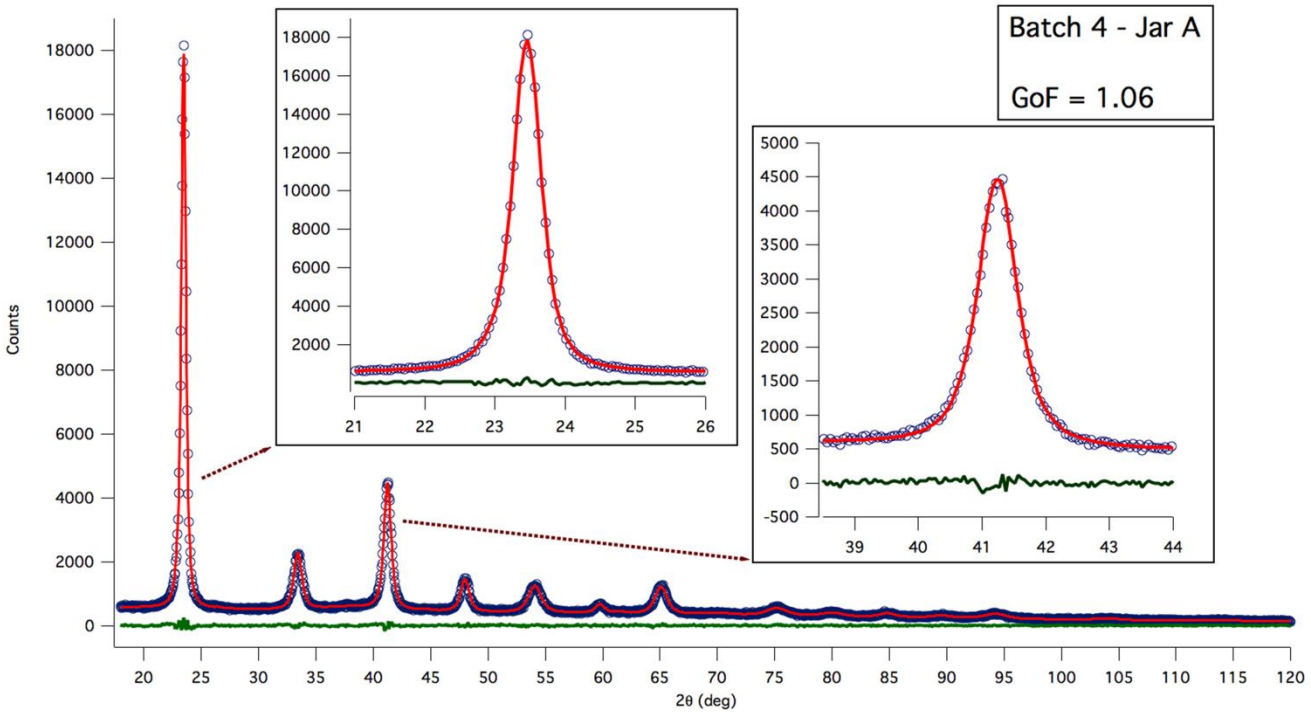

XRD data : MCX beamline, Italian synchrotron ELETTRA

Rebuffi et al., Sci. Reports 6 (2016) 20712

DIFFRACTION FROM NANOCRYSTALLINE *POWDER*

High-energy grinding (ball-milling) of an iron alloy powder: AstaloyTM Fe1.5Mo

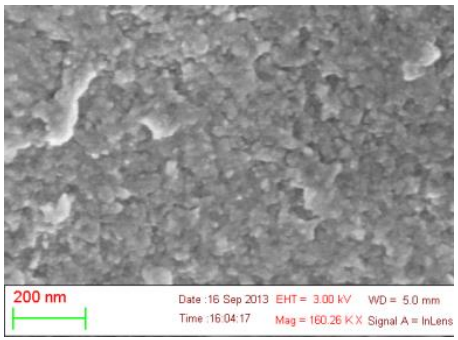

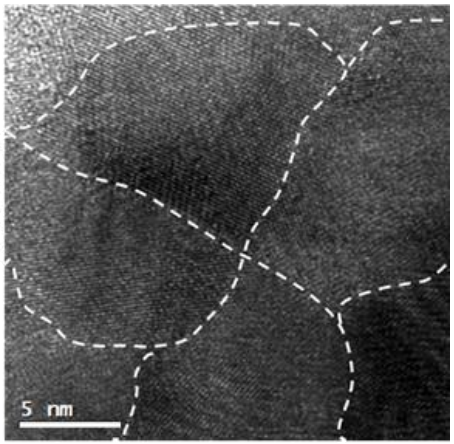

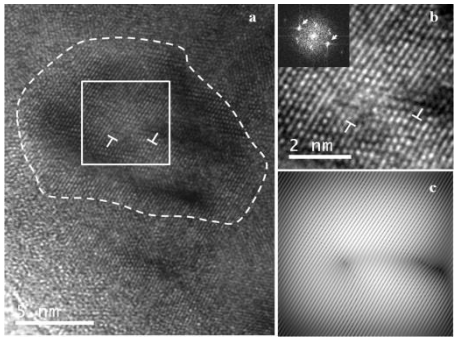

$$I_{hkl}(s) \propto |F|^2 \int A^S(L) A^D_{hkl}(L) T^{IP}(L) e^{2\pi i s L} dL$$

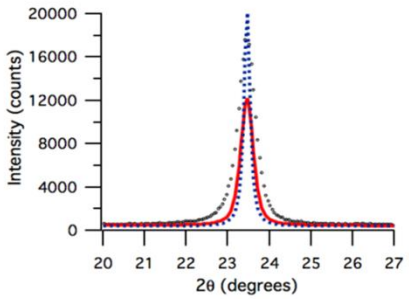

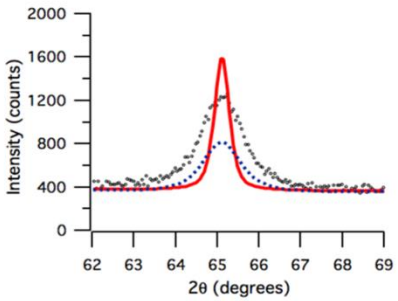

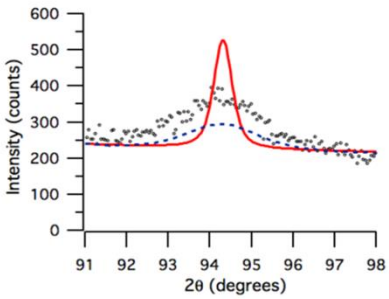

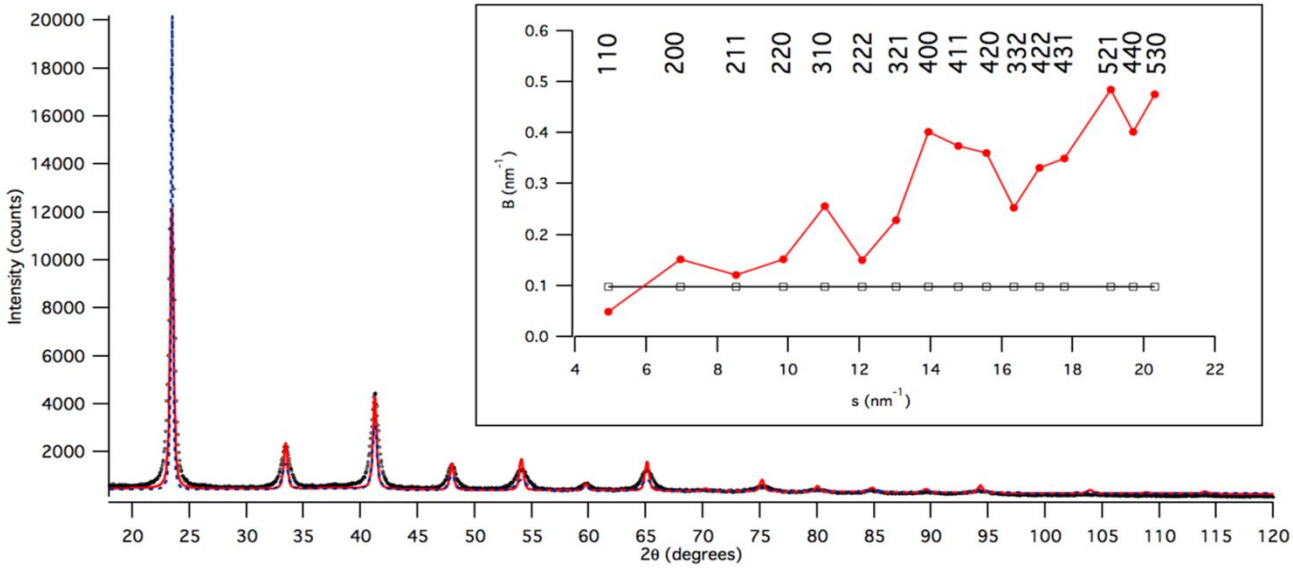

XRD data : MCX beamline, Italian synchrotron ELETTRA

Rebuffi et al., Sci. Reports 6 (2016) 20712

DIFFRACTION FROM NANOCRYSTALLINE *POWDER*

High-energy grinding (ball-milling) of an iron alloy powder: AstaloyTM Fe1.5Mo

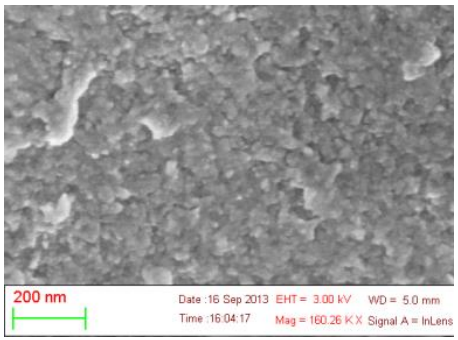

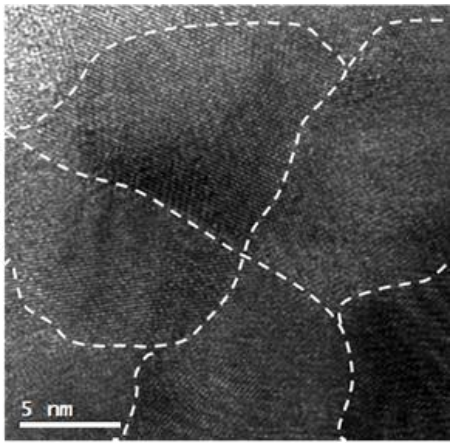

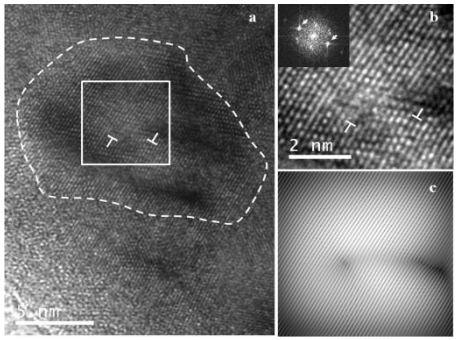

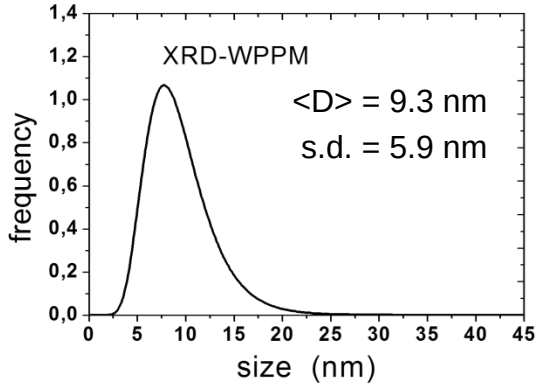

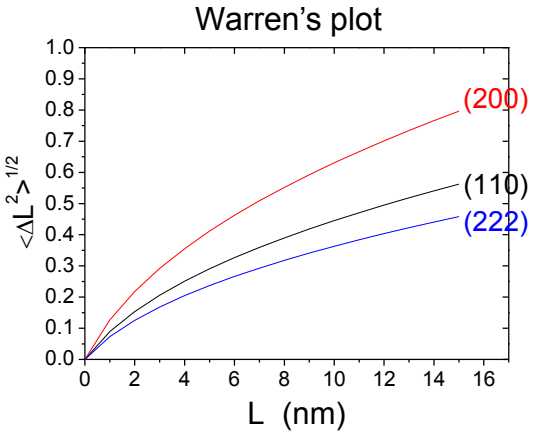

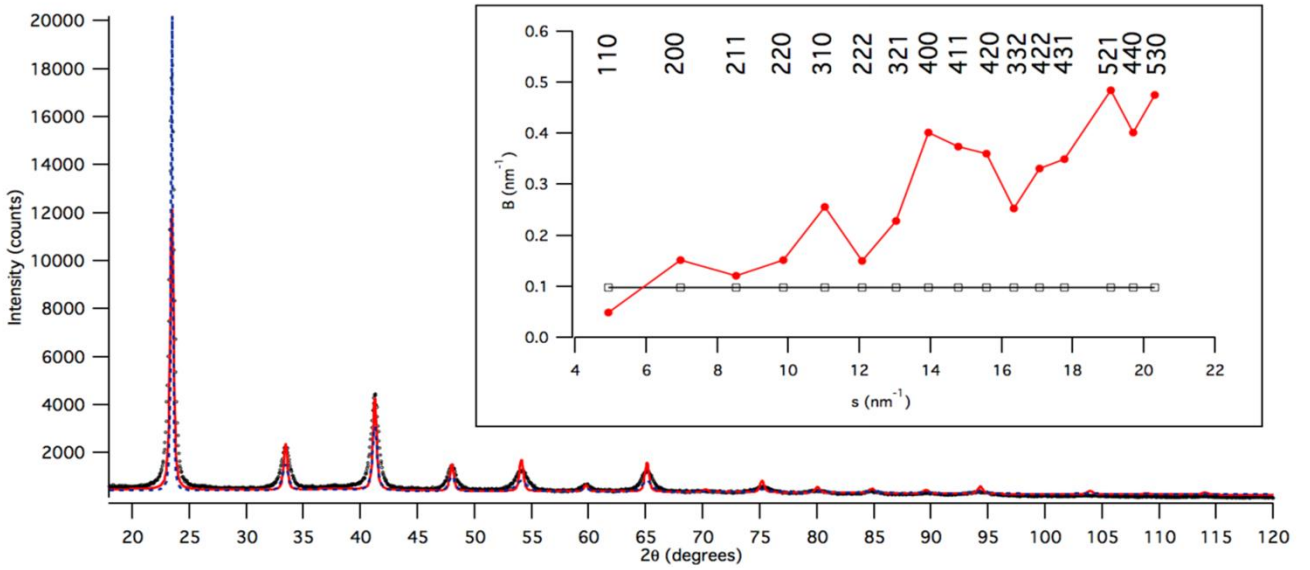

XRD data : MCX beamline, Italian synchrotron ELETTRA

Rebuffi et al., Sci. Reports 6 (2016) 20712

DIFFRACTION FROM NANOCRYSTALLINE *POWDER*

High-energy grinding (ball-milling) of an iron alloy powder: AstaloyTM Fe1.5Mo

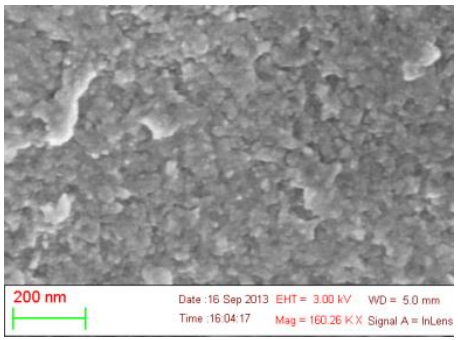

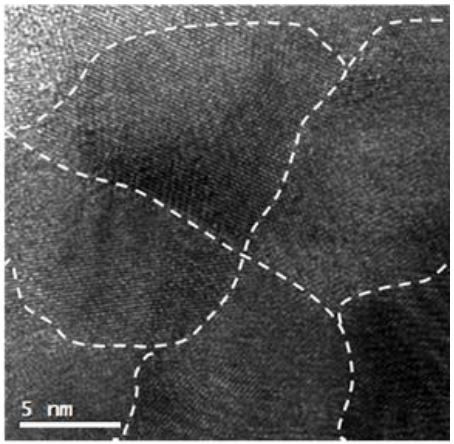

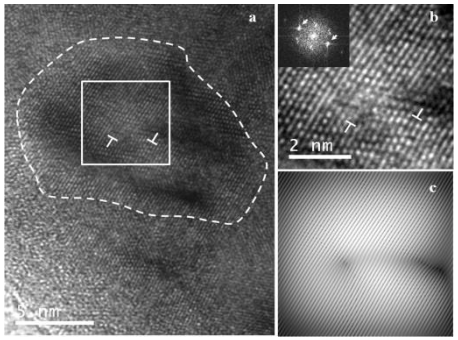

$$< \Delta L_{hkl}{}^2 >= \frac{\rho \bar{C}_{\{hkl\}} b^2}{4\pi} L^2 f^*\left(L/R_e\right)$$

ρ – average dislocation density

$\bar{C}_{\{hkl\}}$ – average contrast factor

b – Burgers vector modulus

R_e – effective outer cut-off radius

f^* – Wilkens' function

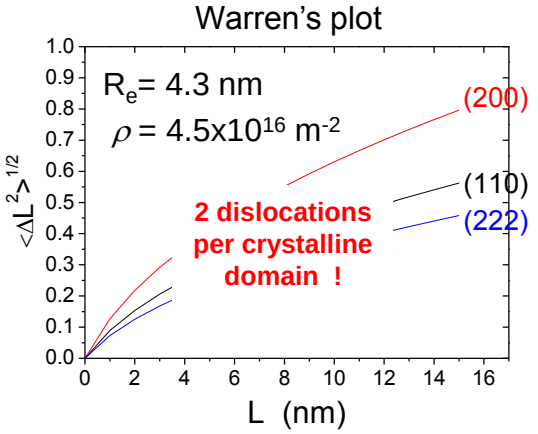

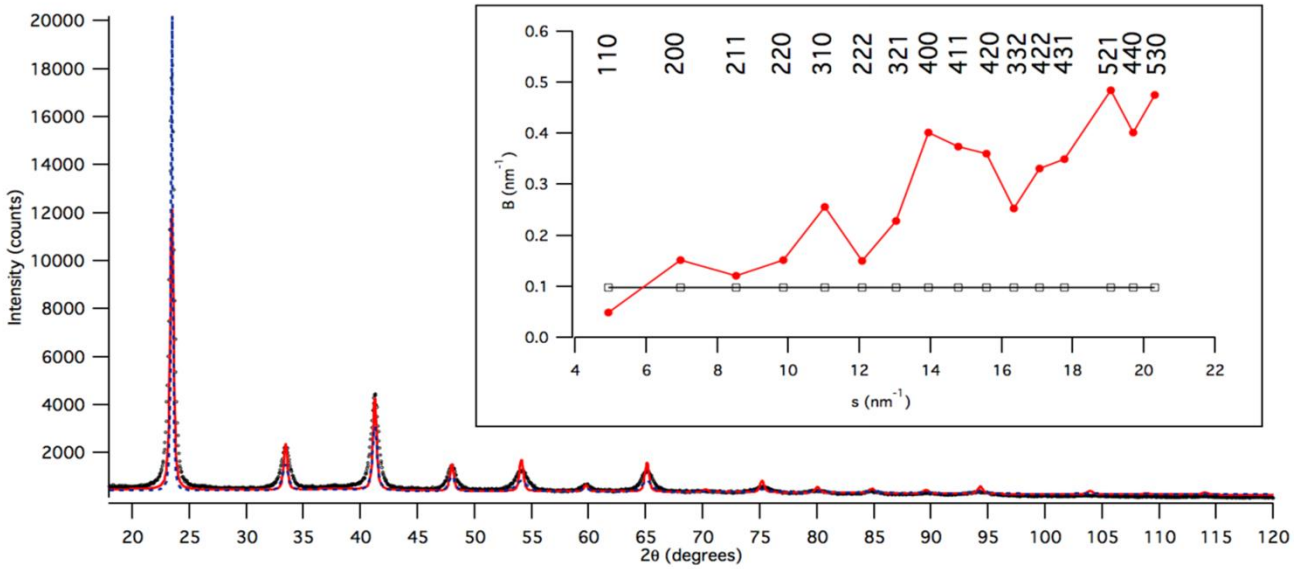

XRD data : MCX beamline, Italian synchrotron ELETTRA

Rebuffi et al., Sci. Reports 6 (2016) 20712

DIFFRACTION FROM NANOCRYSTALLINE *POWDER*

Understanding XRD line profile analysis result by Molecular Dynamics simulations

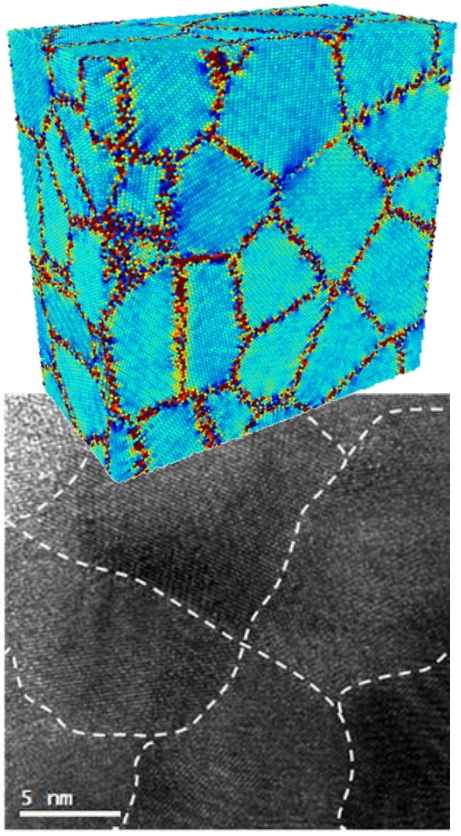

Molecular Dynamics (MD) simulation

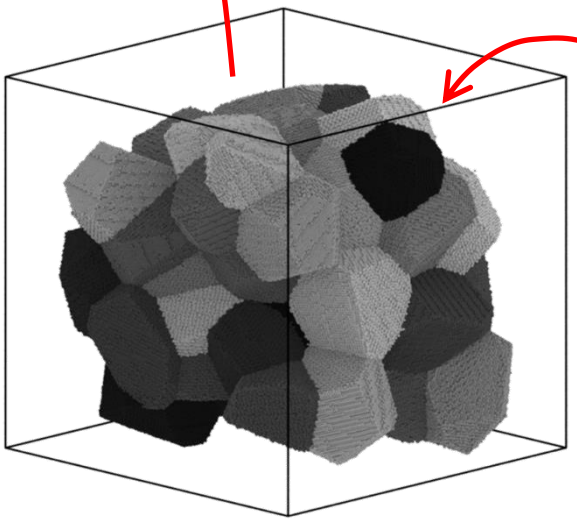

atomistic model by space tessellation

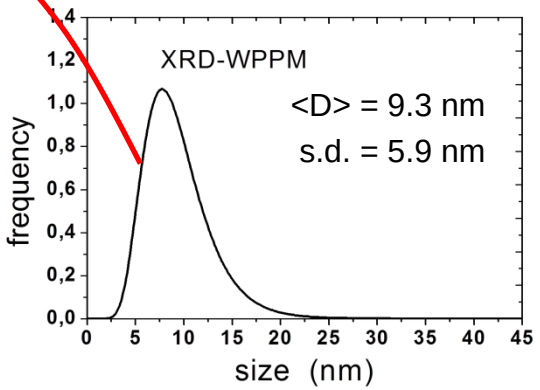

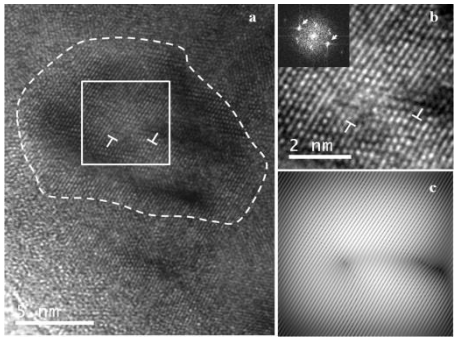

Rebuffi et al., Sci. Reports 6 (2016) 20712

DIFFRACTION FROM NANOCRYSTALLINE *POWDER*

Understanding XRD line profile analysis result by Molecular Dynamics simulations

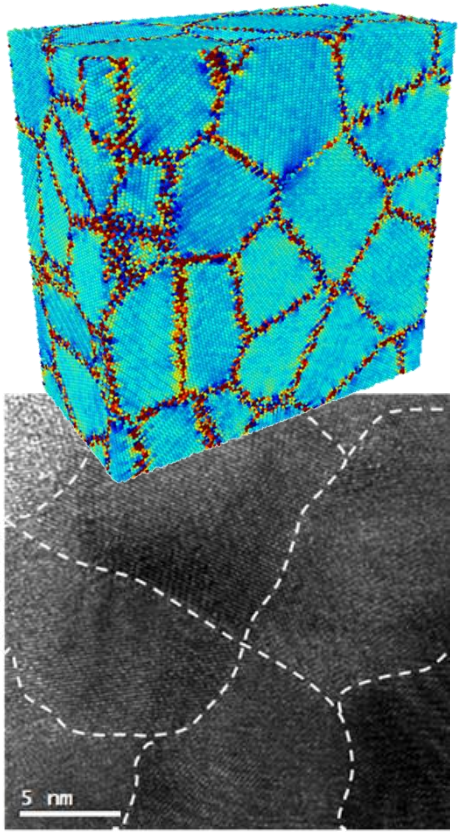

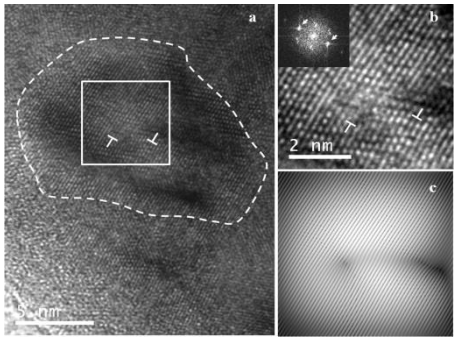

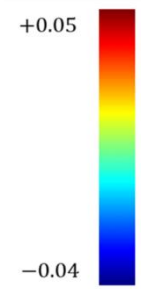

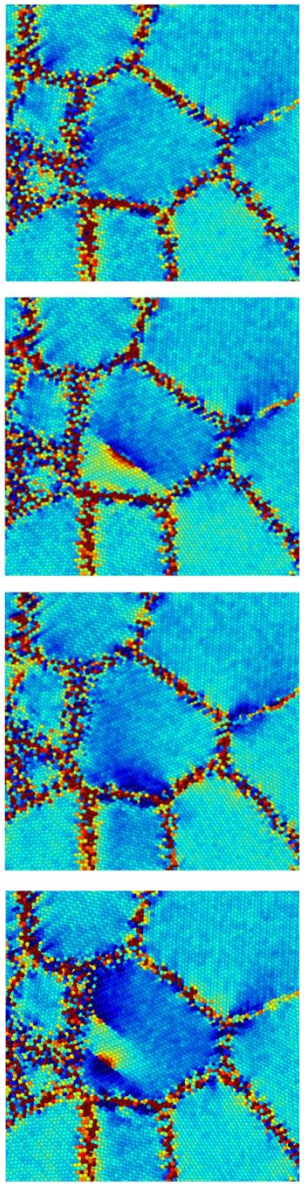

grain-grain interaction only

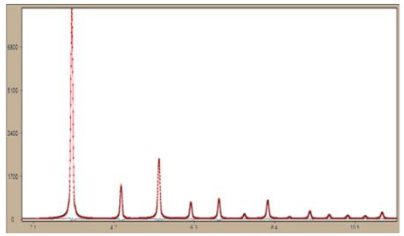

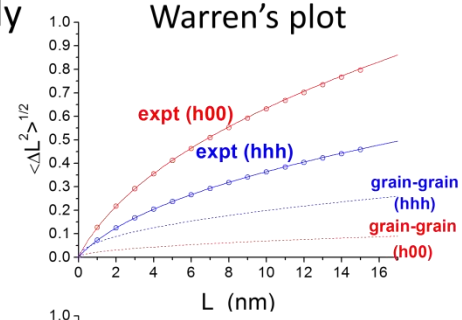

1 edge dislocation

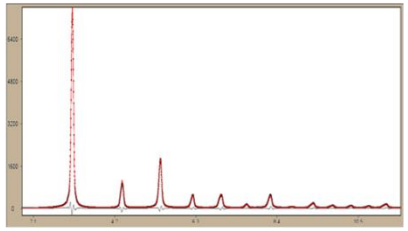

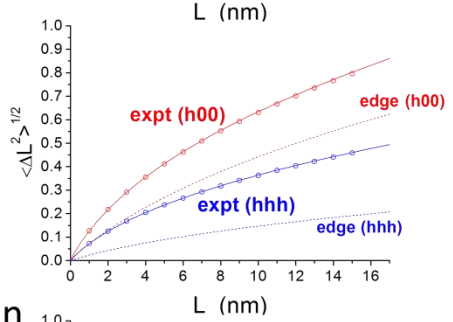

1 unstable edge dislocation

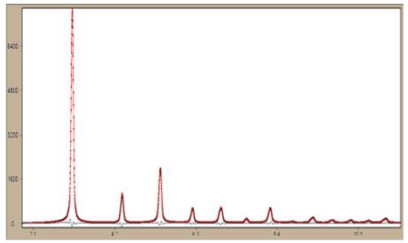

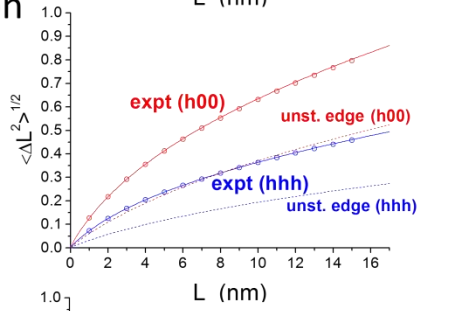

1 edge dislocation dipole

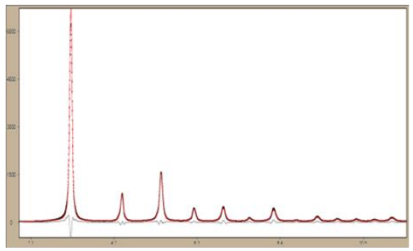

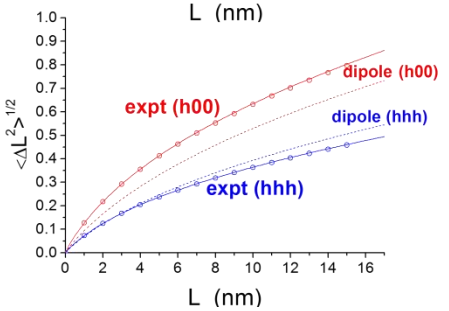

Rebuffi et al., Sci. Reports 6 (2016) 20712

DIFFRACTION FROM NANOCRYSTALLINE *POWDER*

Temperature Diffuse Scattering – TDS

Perfect Static Lattice

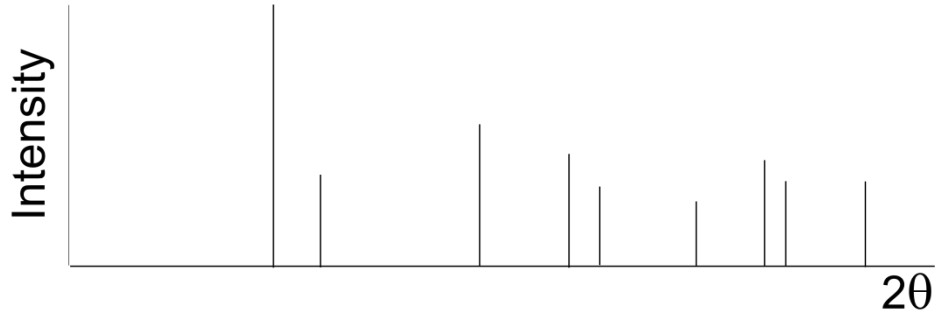

Random Atomic Motion

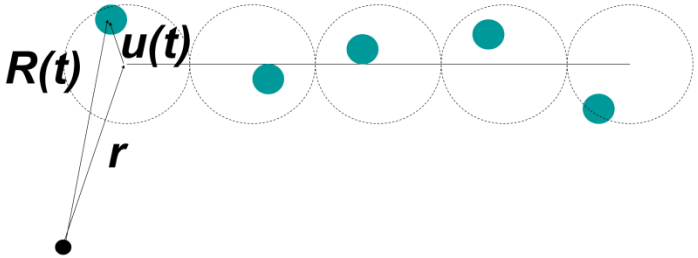

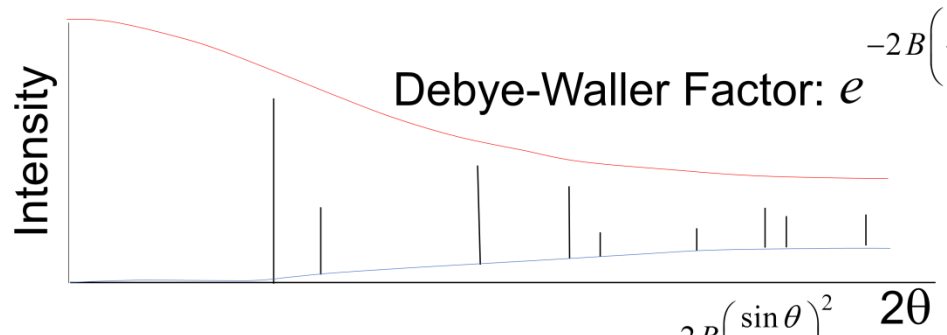

Debye-Waller Factor: $e^{-2B\left(\frac{\sin\theta}{\lambda}\right)^2}$

Debye TDS: $1-e^{-2B\left(\frac{\sin\theta}{\lambda}\right)^2}$

Correlated Atomic Motion

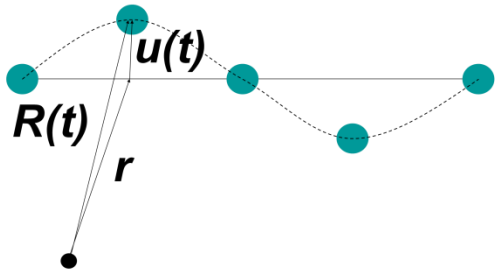

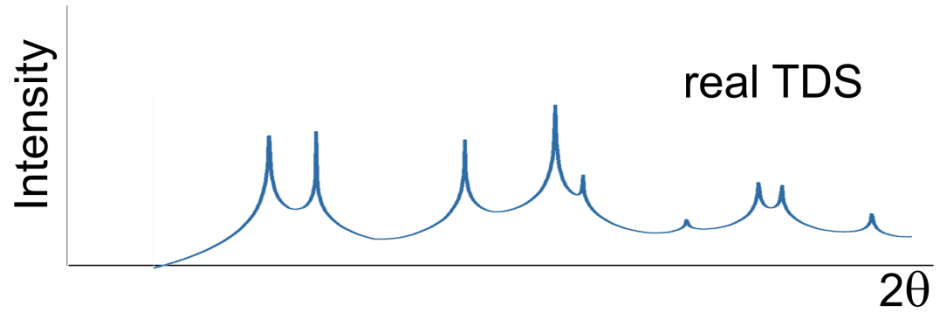

DIFFRACTION FROM NANOCRYSTALLINE *POWDER*

Temperature Diffuse Scattering – TDS in small crystals

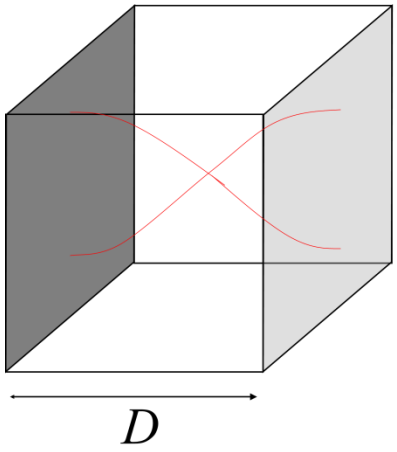

$$\lambda_{\max} \approx 2D$$

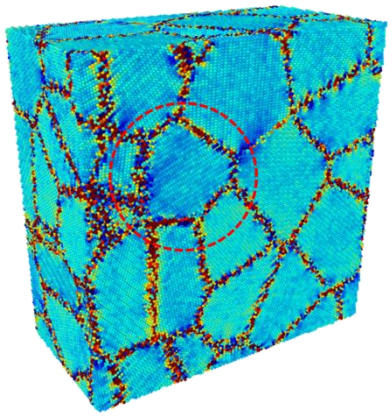

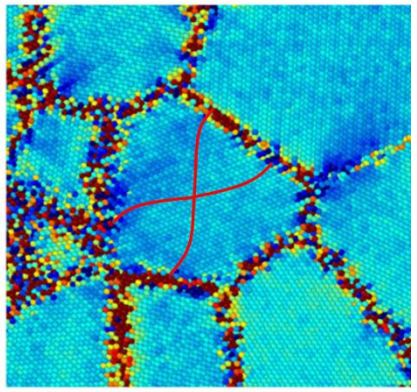

$$\omega_{\min} = 2\pi c_s(\omega) / \lambda_{\max} = \omega_{\min}(D)$$

small λ_{max} → truncation of TDS peaks

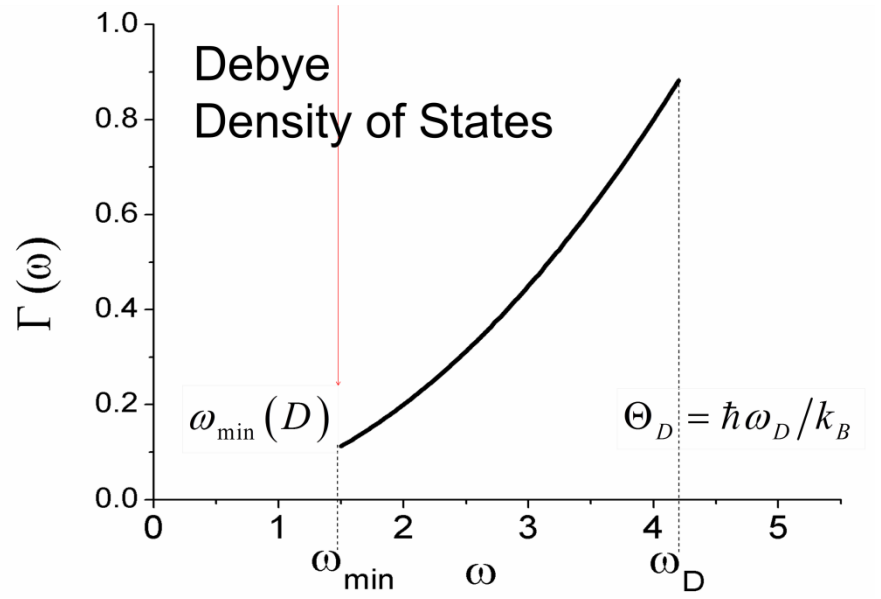

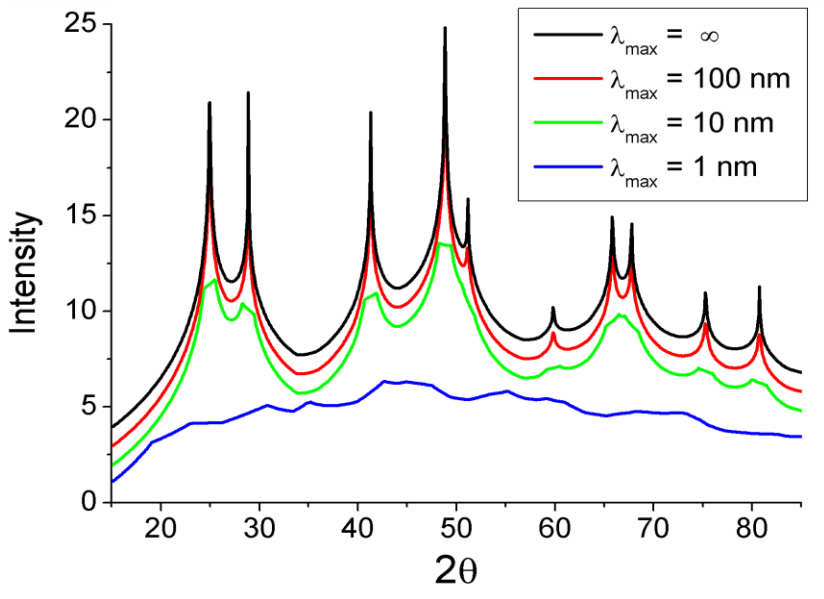

DIFFRACTION FROM NANOCRYSTALLINE *POWDER*

TDS in ball-milled FeMo nanocrystals: static and dynamic contributions

Argonne 11bm, 30keV – 100, 200, 300K

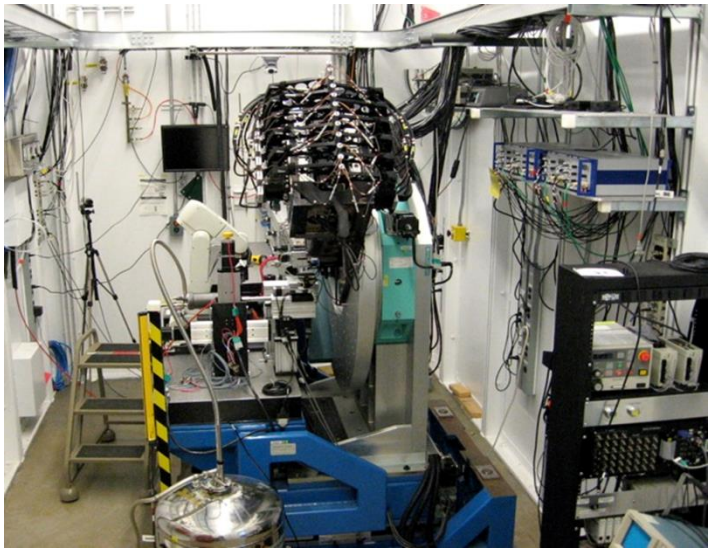

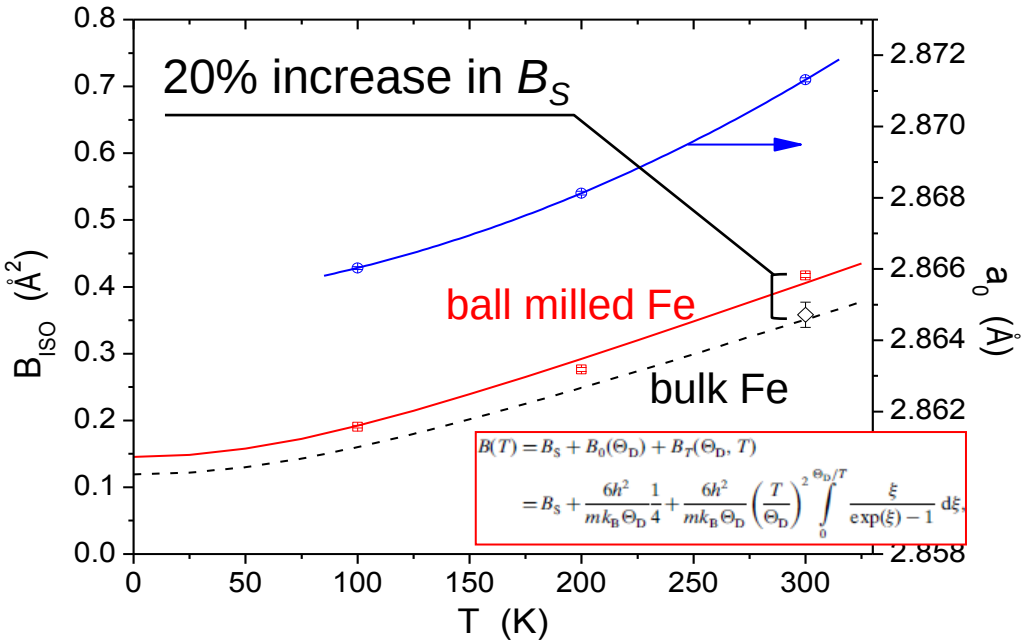

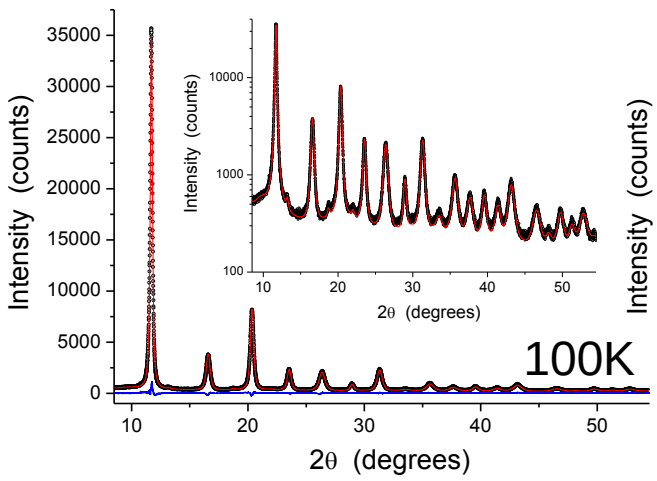

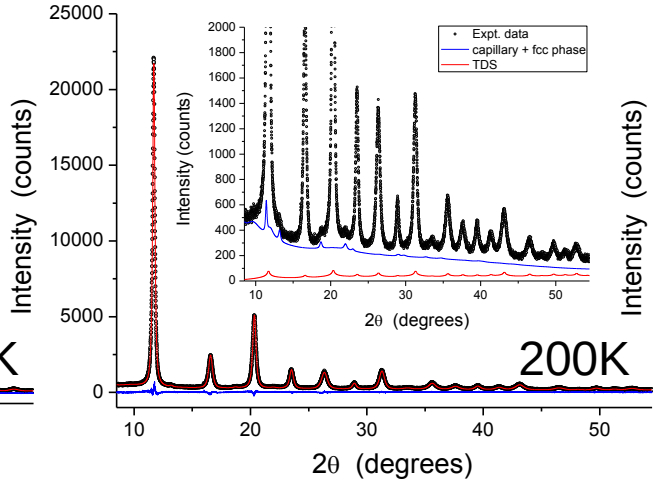

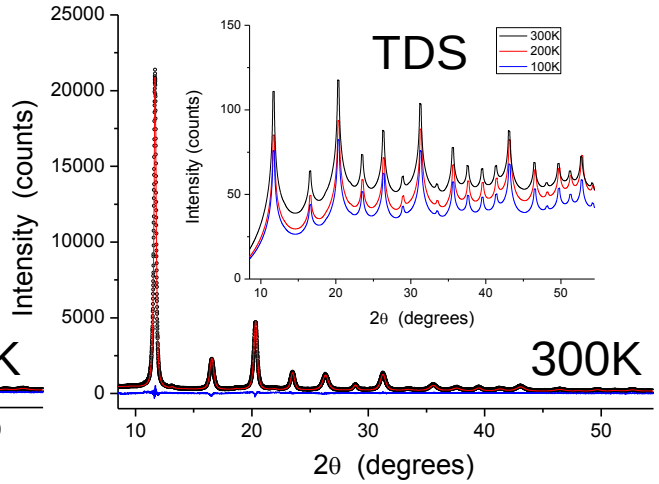

P. Scardi et al. J. Appl. Cryst. 50 (2017) 508

DIFFRACTION FROM NANOCRYSTALLINE *POWDER*

EXAFS & XRD : Mean Square Displacement (MSRD, MSD) and DCF

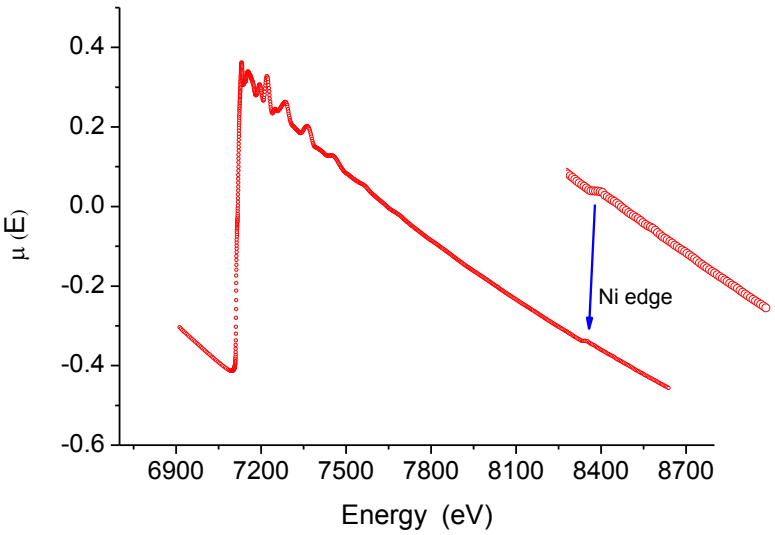

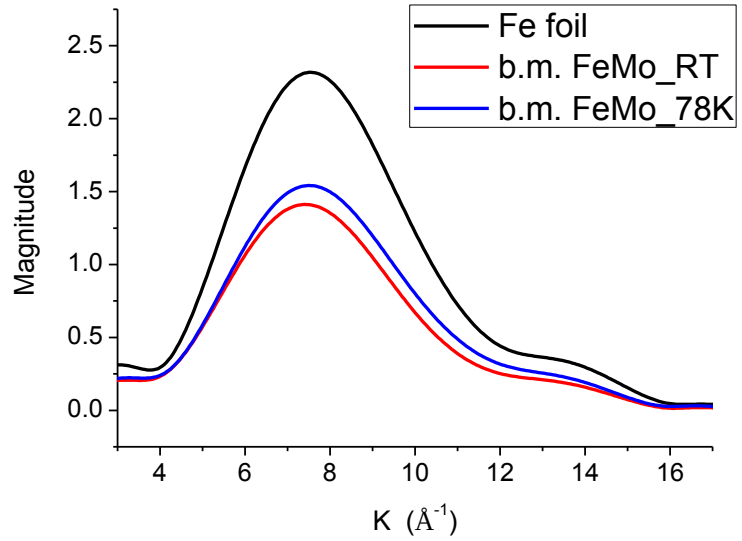

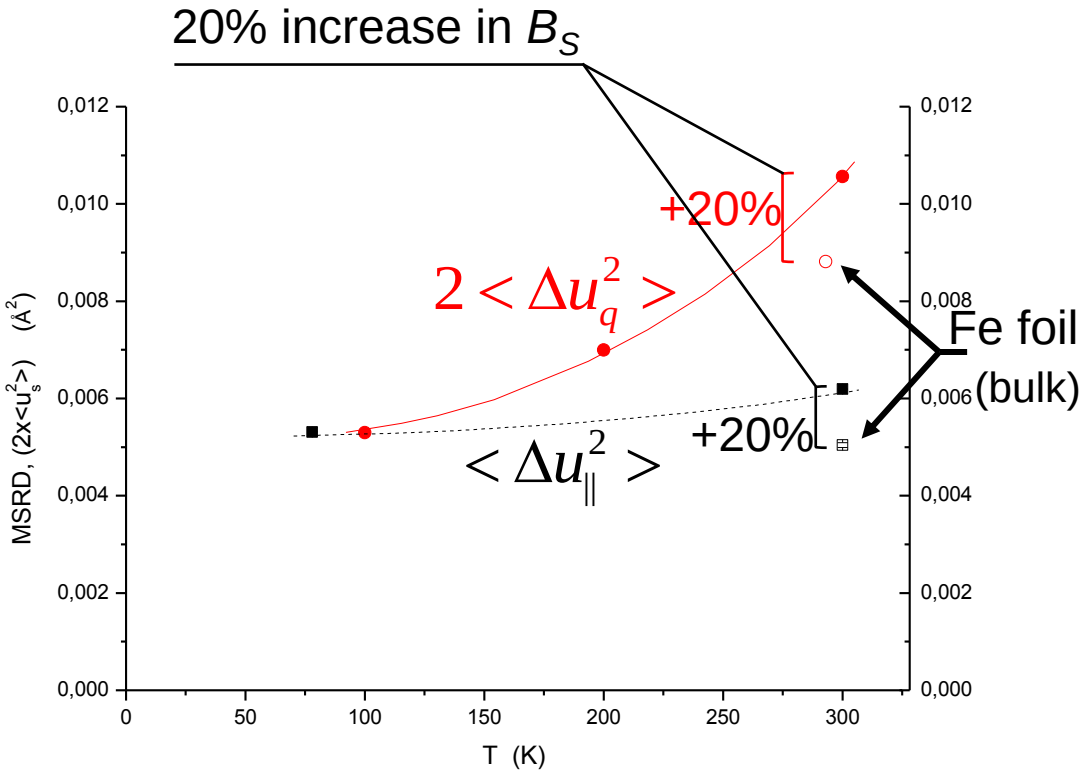

- EXAFS Debye-Waller parm. $< \Delta u_{\|}^2 >$: 1° coordination shell
- XRD Debye-Waller parm. $< \Delta u_q^2 >$=B/8π² : average over whole crystal

$$< \Delta u_{\|}^2 >= MSRD = 2 \times < \Delta u_q^2 > - DCF$$

P. Scardi et al. J. Appl. Cryst. 50 (2017) 508

DIFFRACTION FROM NANOCRYSTALLINE *POWDER*

What is the main reason for the 20% increase in B_S (static disorder) ?

Molecular Dynamics simulation of a cluster of 50 Fe grains (size distribution from XRD/WPPM)

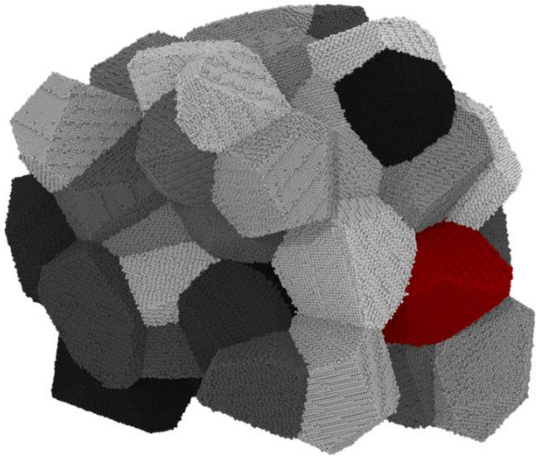

MSD - Mean Square Displacement $< \Delta u_q^2 >$ ($B=8\pi^2 < \Delta u_q^2 >$) results for average-size grain (G5)

	no defects g.b. only	1 edge disloc. and g.b.	vacancies and g.b.
			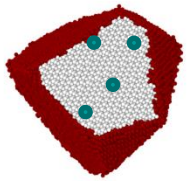
$\Delta B = B_{G5} - B_{bulk}$	22%	22%+ ~2%	22%+ ~0% (<<1%)

P. Scardi et al. J. Appl. Cryst. 50 (2017) 508

FROM SINGLE CRYSTAL TO POWDER DIFFRACTION

1. Traditional reciprocal space approach : sum & average

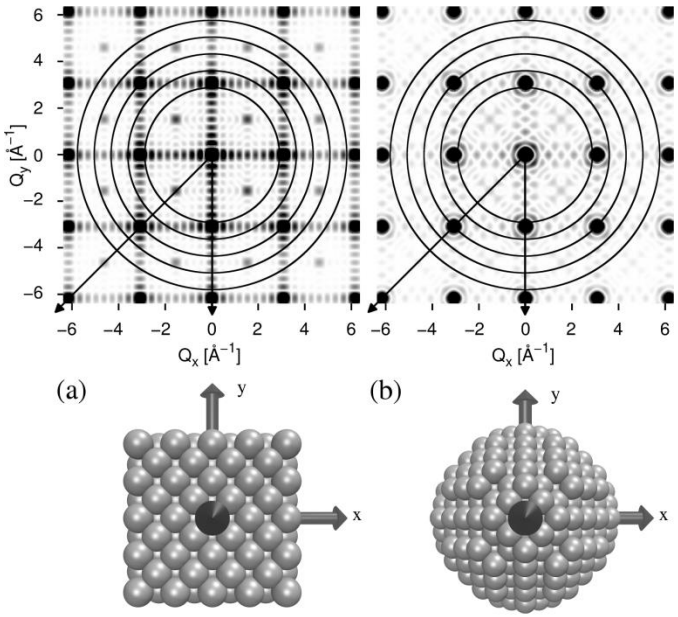

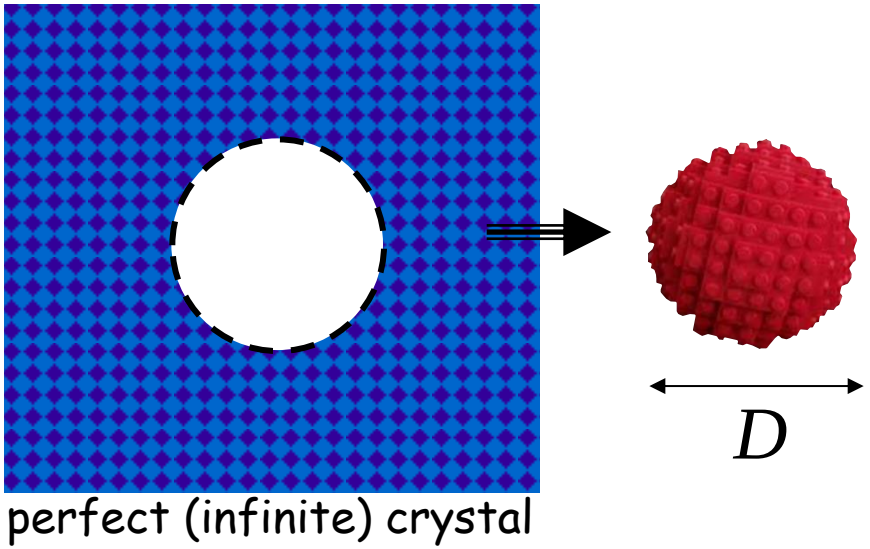

perfect (infinite) crystal

$$I_{sc}(\underline{s}) \propto \sum_m \sum_n f_m f_n^* e^{2\pi i(\underline{S}\cdot\underline{r}_{mn})}$$

$$I_{PD}(s) \propto \frac{\int I_{sc}(\underline{s})\,d\Omega}{4\pi s^2} = |F|^2 \left\{ I^{IP}(s) \otimes I^{S}(s) \otimes I^{D}(s) \otimes I^{F}(s) \otimes I^{APB}(s) \otimes I^{C}(s) \otimes I^{GRS}(s) \ldots \right\}$$

DIFFRACTION FROM NANOCRYSTALLINE MATERIALS

☹ real nanocrystals are complex objects

non-crystallographic (e.g. multiply twinned) nanoparticles, 2D and highly disordered layer systems:

- translational symmetry: not verified
- large strain / misfit - complex local atomic arrangement

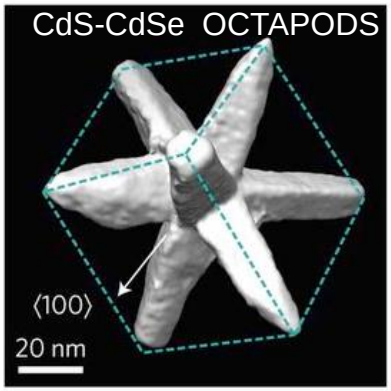

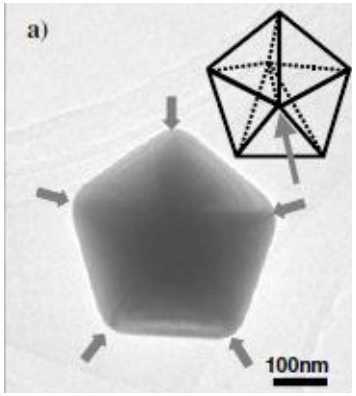

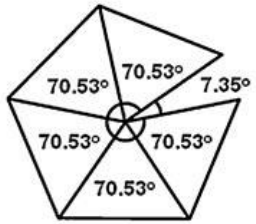

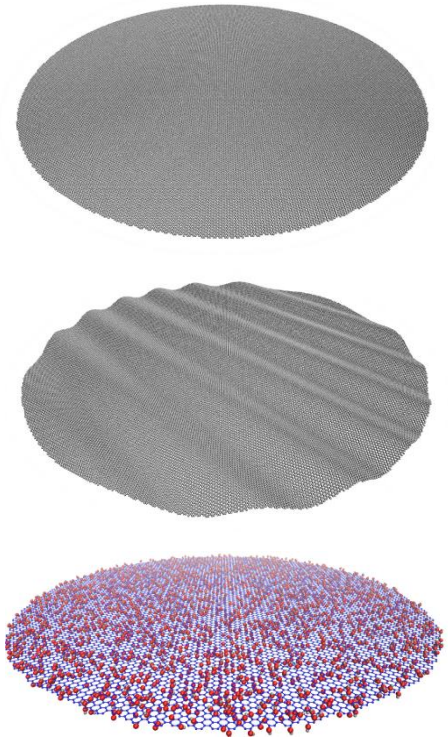

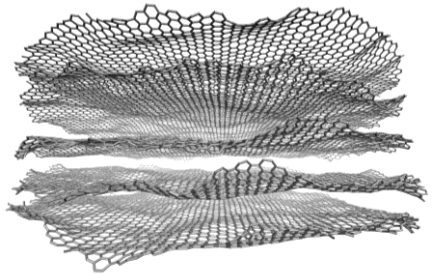

2. Direct (real) space approach : average & sum

$$I_{PD}(s) = \frac{\int \sum_m \sum_n f_m f_n^* e^{2\pi i(\underline{s}\cdot\underline{r}_{mn})} d\Omega}{4\pi s^2}$$

2. Direct (real) space approach : average & sum

$$I_{PD}(s) = \frac{|f|^2 \sum_m \sum_n \int e^{2\pi i(\underline{s}\cdot\underline{r}_{mn})} d\Omega}{4\pi s^2}$$

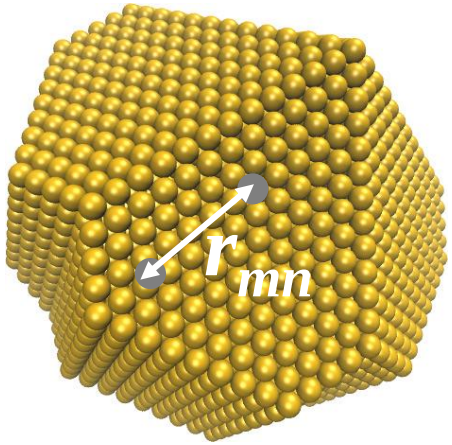

$$\left\langle e^{2\pi i(\underline{s}\cdot\underline{r}_{mn})} \right\rangle = \frac{1}{4\pi r_{mn}^2} \int_0^{\pi} e^{2\pi i s r_{mn}\cos\phi} 2\pi r_{mn}^2 \sin\phi d\phi = \frac{\sin(2\pi s r_{mn})}{2\pi s r_{mn}}$$

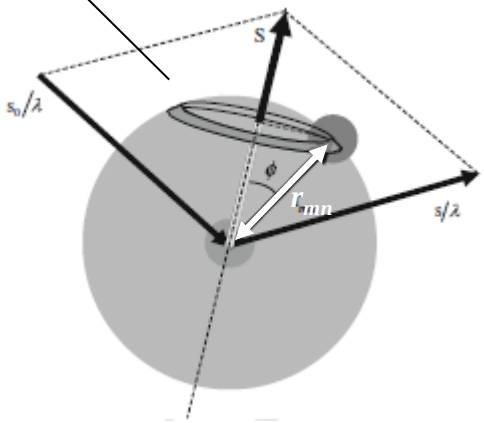

$$I_{PD}(s) = |f|^2 \sum_m \sum_n \frac{\sin(2\pi s r_{mn})}{2\pi s r_{mn}}$$

Debye Scattering Equation (DSE)

DSE APPLICATION TO NON-CRYSTALLOGRAPHIC NPs

Debye Scattering Equation (DSE)

$$I_{PD}(s) = |f|^2 \sum_m \sum_n \frac{\sin(2\pi s r_{mn})}{2\pi s r_{mn}}$$

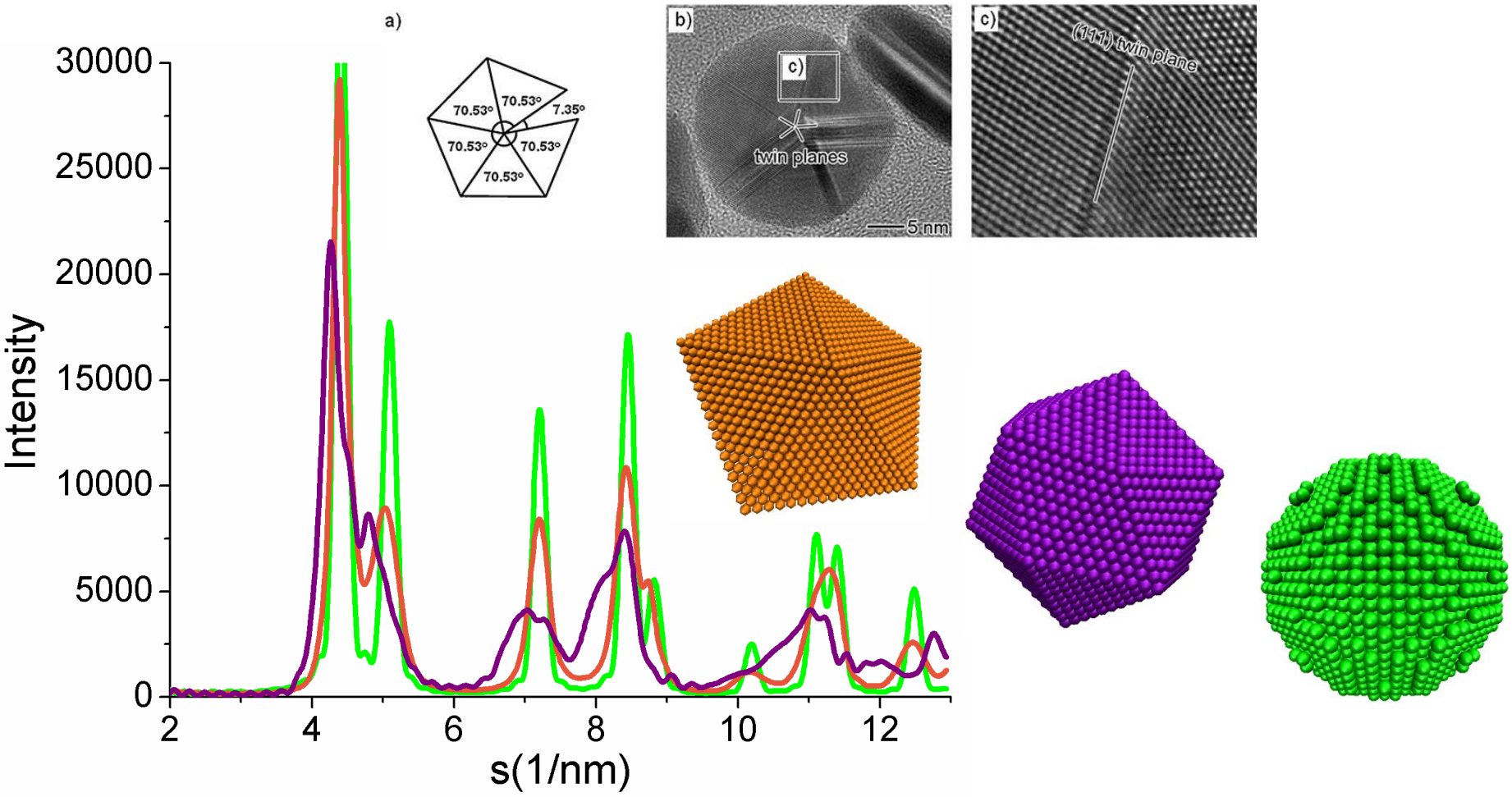

Debye Scattering Equation (DSE)

$$I_{PD}(s) = |f|^2 \sum_m \sum_n \frac{\sin(2\pi s r_{mn})}{2\pi s r_{mn}}$$

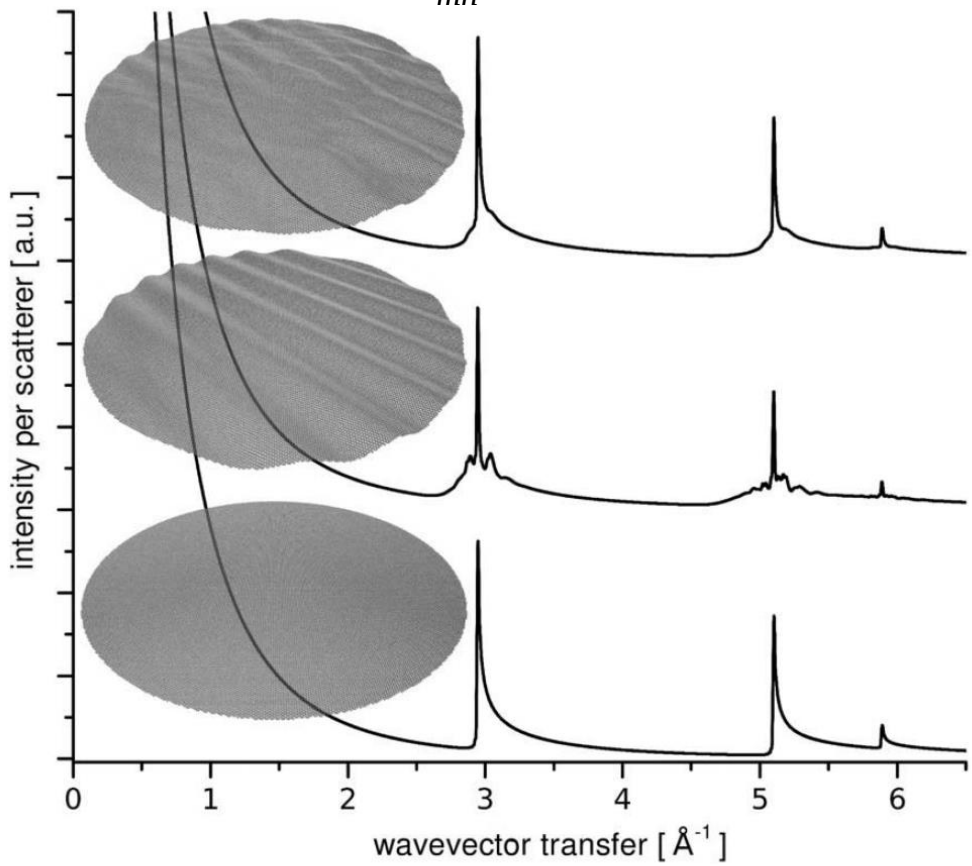

Figure 7
Powder patterns for graphene disks of diameter D = 500 Å. Regular, flat graphene (bottom), undulate graphene (middle) and graphene with a random roughness (top). See text for details.

L. Gelisio et al., J. Appl. Cryst. 43 (2014) 647

DSE APPLICATION TO GRAPHENE AND RELATED MATERIALS

Debye Scattering Equation (DSE)

$$I_{PD}(s) = |f|^2 \sum_m \sum_n \frac{\sin(2\pi s r_{mn})}{2\pi s r_{mn}}$$

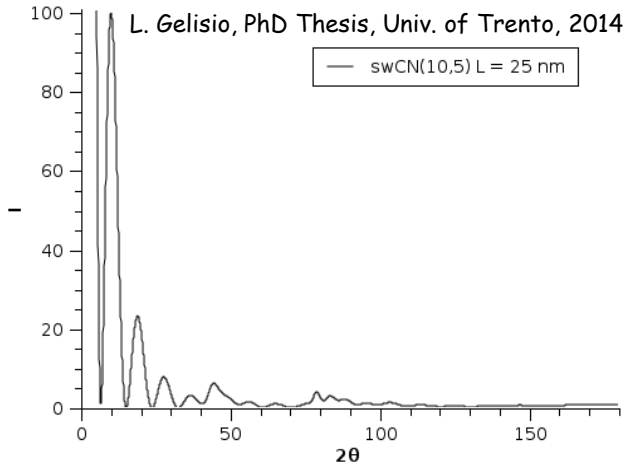

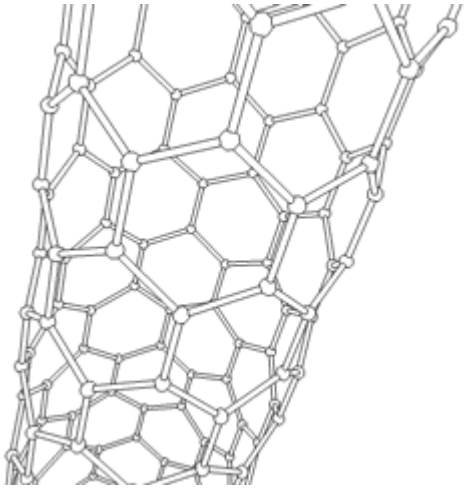

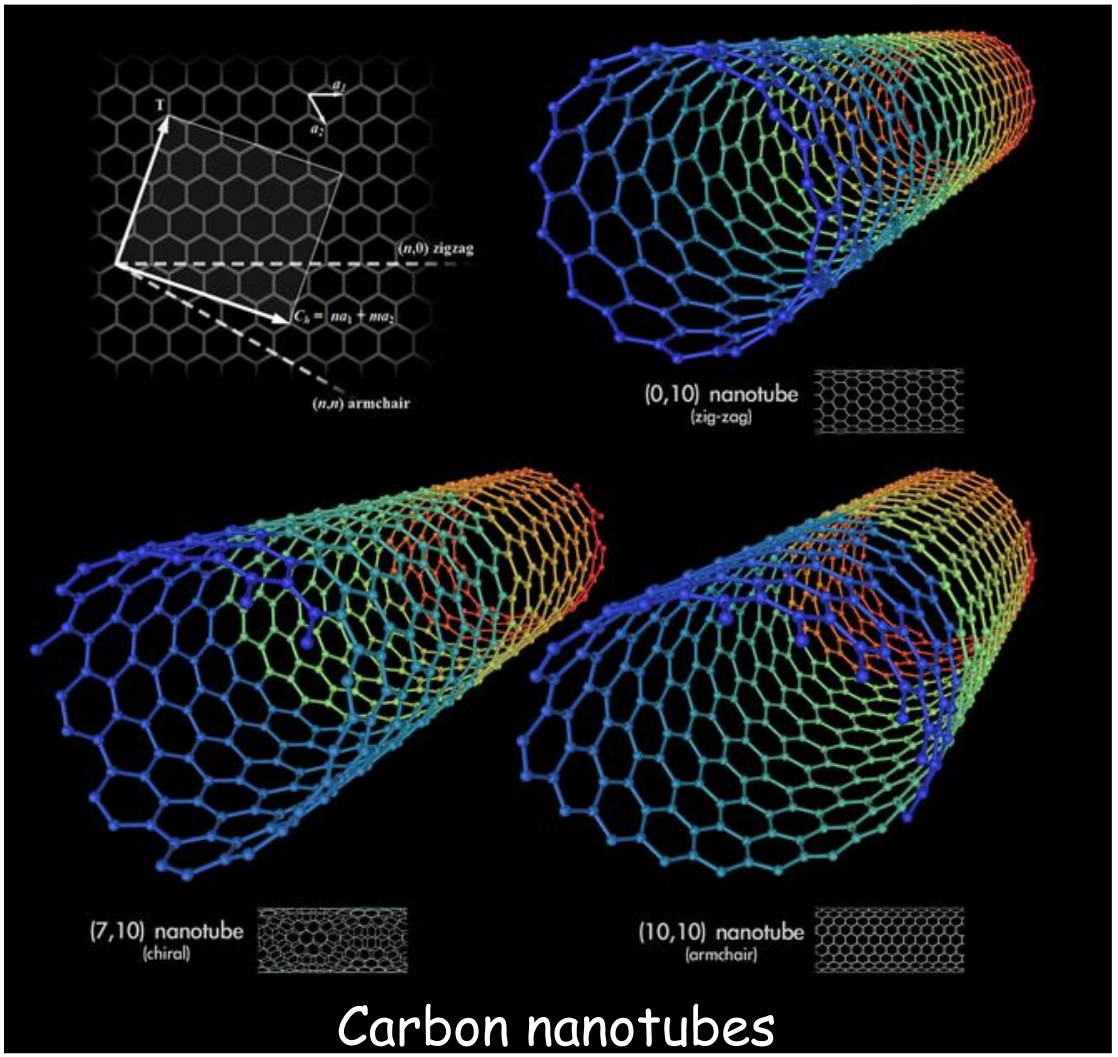

DSE CALCULATION BY ATOMIC DISTANCE HISTOGRAM

Debye Scattering Equation (DSE)

$$I_{PD}(s) = |f|^2 \sum_m \sum_n \frac{\sin(2\pi s r_{mn})}{2\pi s r_{mn}} \equiv |f|^2 \sum_{mn} B_{mn} \frac{\sin(2\pi s r_{mn})}{2\pi s r_{mn}}$$

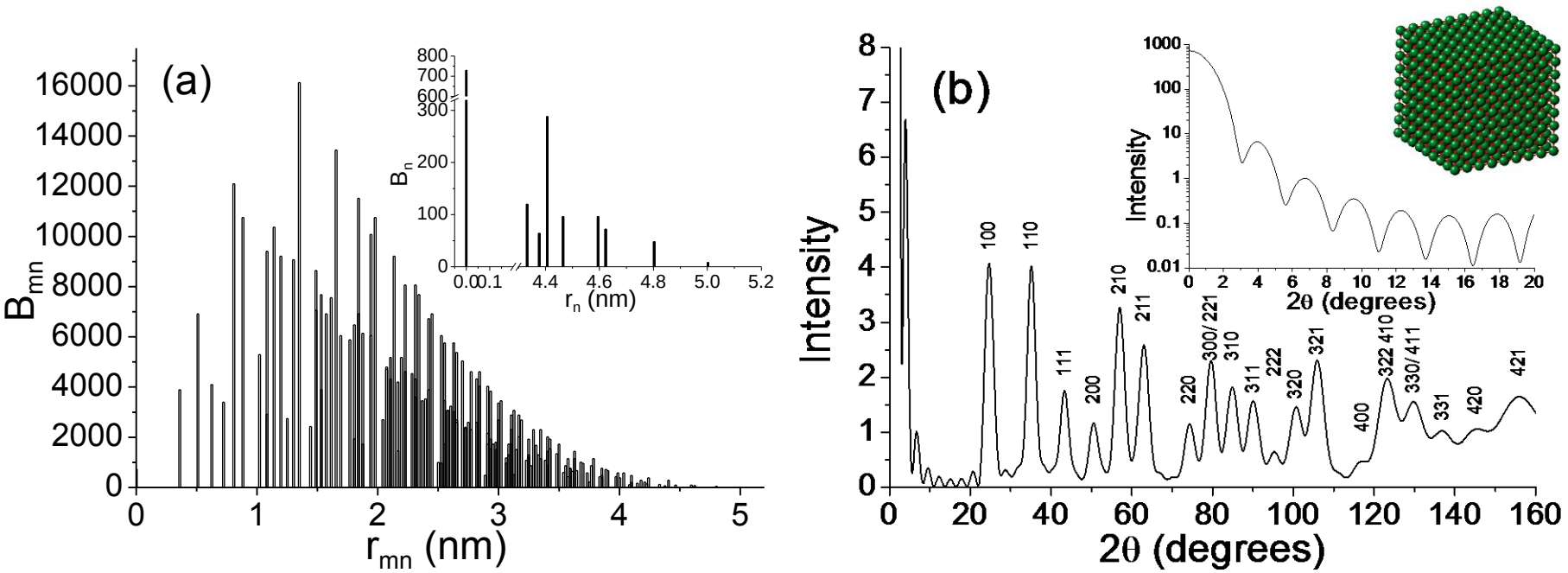

Atomic distance histogram (B_{mn}) for a cubic crystal with 8x8x8 sc unit cells (a) and corresponding powder pattern according to $I_{PD}(s)$, with f=1, unit cell parameter, a_0=0.361 nm (b).
In: P. Scardi & L. Gelisio, "Diffraction from nanocrystalline materials", Chapter XVIII.

PAIR DISTRIBUTION FUNCTION (PDF)

Zernike & Prins (1927): for amorphous specimens, volume *V*, *N* atoms, the *radial distribution function* (RDF) is:

$$RDF(r) = 4\pi r^2 \rho(r) \cong 4\pi r^2 \rho_0 + 8\pi r \int_0^\infty s\left[\frac{I(s)}{Nf^2} - 1\right] Sin(2\pi sr)\, ds$$

intensity in absolute units:

$$\left[\frac{I(s)/N - f^2}{f^2}\right] \rightarrow = \left[\frac{(a-d)-c}{c}\right]$$

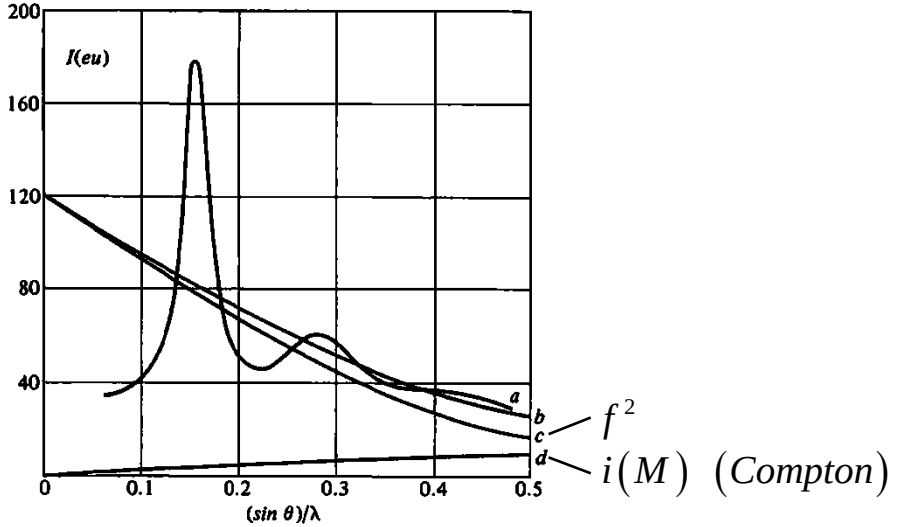

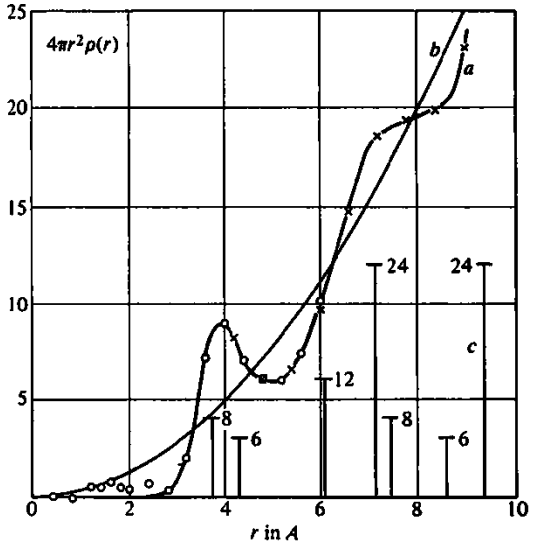

Fig. 10.4 (a) Total intensity curve for liquid sodium in electron units per atom, unmodified plus modified. (b) Total independent scattering per atom. (c) Independent unmodified scattering per atom f^2. (d) Modified scattering per atom $i(M)$.

Fig. 10.6 (a) The radial distribution function $4\pi r^2\rho(r)$ for liquid sodium. (b) The average density curve $4\pi r^2\rho_a$. (c) The distribution of neighbors in crystalline sodium.

PDF AND SYNCHROTRON RADIATION

SR is mandatory to improve resolution!

1950

1999

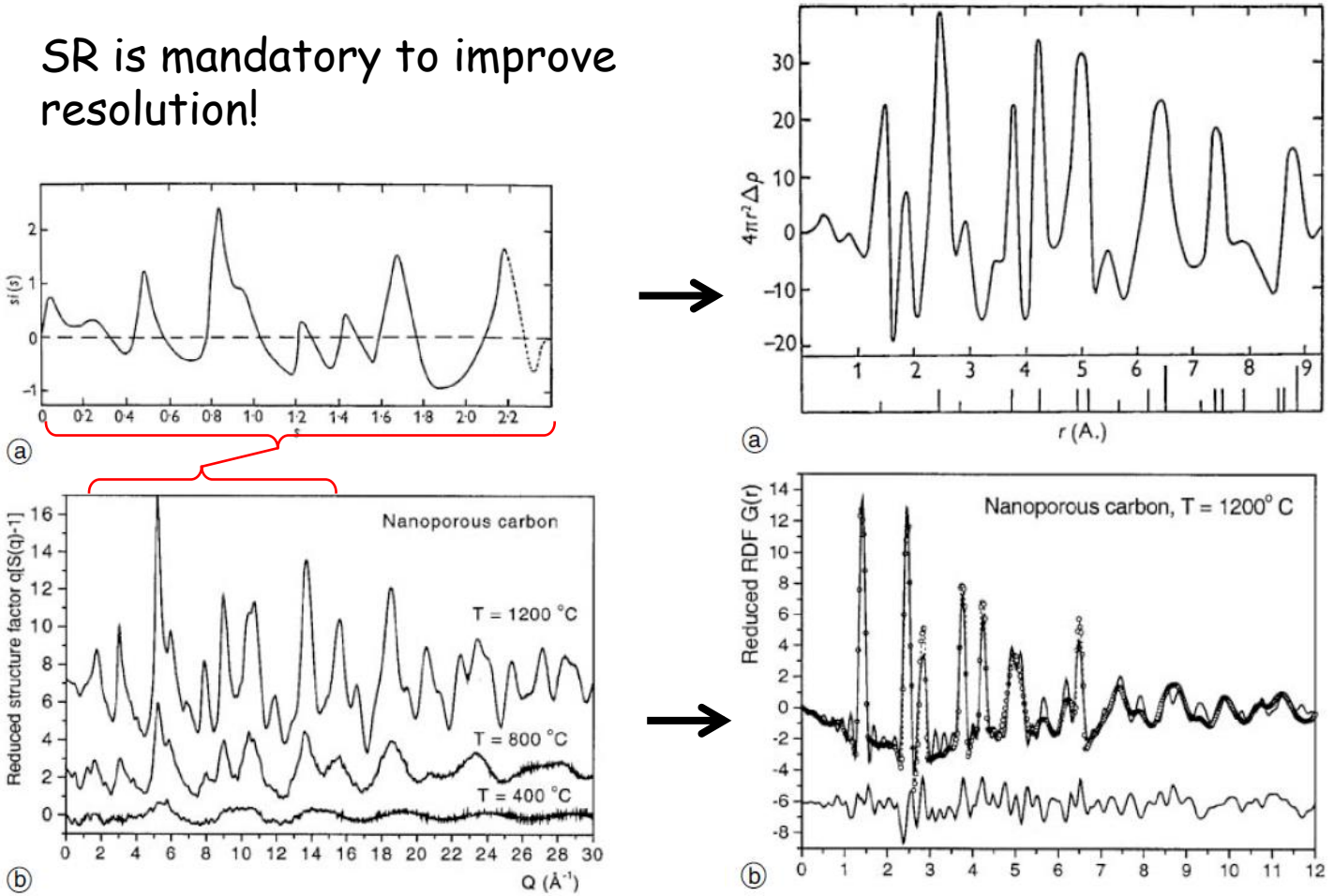

Fig. 1. Comparison of data from disordered carbon from (**a**) 1950 (Franklin, 1950) and (**b**) 1999 (Petkov et al., 1999a). This figure shows that both $i(Q) = Q[S(Q) - 1]$ curves are of essentially equal quality but the 1999 data in the lower panel extend over a much greater range of Q. Note the different scales; Q in the 1999 data and s in the 1950 data are related by $Q = 2\pi s$. The Fourier transforms of the data can be compared in Fig. 2.

Fig. 2. Comparison of data from disordered carbon from (**a**) 1950 (Franklin, 1950) and (**b**) 1999 (Petkov et al., 1999a). The PDFs obtained by Fourier transforming the two data-sets shown in Fig. 1 are shown in the top (1950 data) and bottom (1999 data) panels, respectively. Note that when data are measured over a sufficiently wide range of Q termination ripples, evident as a spurious peak at $r = 2.5$ Å in the 1950 PDF, for example, are not a problem.

→ S. J. L. Billinge, Z. Kristallogr. 219 (2004) 117

PAIR DISTRIBUTION FUNCTION (PDF)

$RDF(r) = 4\pi r^2 \rho(r)$ *radial distribution function*

$G(r) = 4\pi r[\rho(r) - \rho_0]$ *reduced radial distribution function*

$g(r) = \rho(r)/\rho_0$ *pair distribution function - PDF*

$$= 1 + \frac{2}{\rho_0 r}\int_0^\infty s[S(s)-1]\,Sin(2\pi sr)\,ds \qquad S(s) = \frac{I(s)}{Nf^2}$$

→ S. J. L. Billinge, Z. Kristallogr. 219 (2004) 117

PDF AND SYNCHROTRON RADIATION

SR is mandatory to improve resolution!

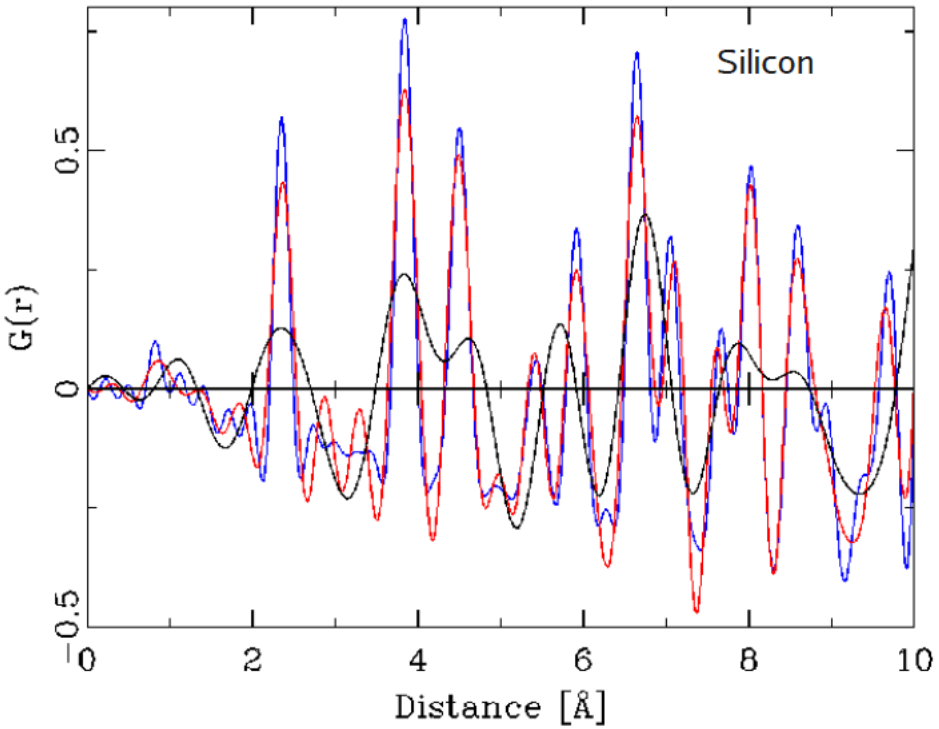

PSI high resolution data
Silicon

Q_{max} = 21. Å^{-1}
Synchrotron

Q_{max} = 15. Å^{-1}
Mo-Kα

Q_{max} = 7. Å^{-1}
Cu-Kα

Width of PDF maxima decreases with increasing Q_{max}

Reasonable for Q_{max} > 20 Å^{-1}

→ Courtesy of R. Neder

PDF OF NANOPARTICLE SYSTEMS

Effect of finite size and shape of the nanoparticle

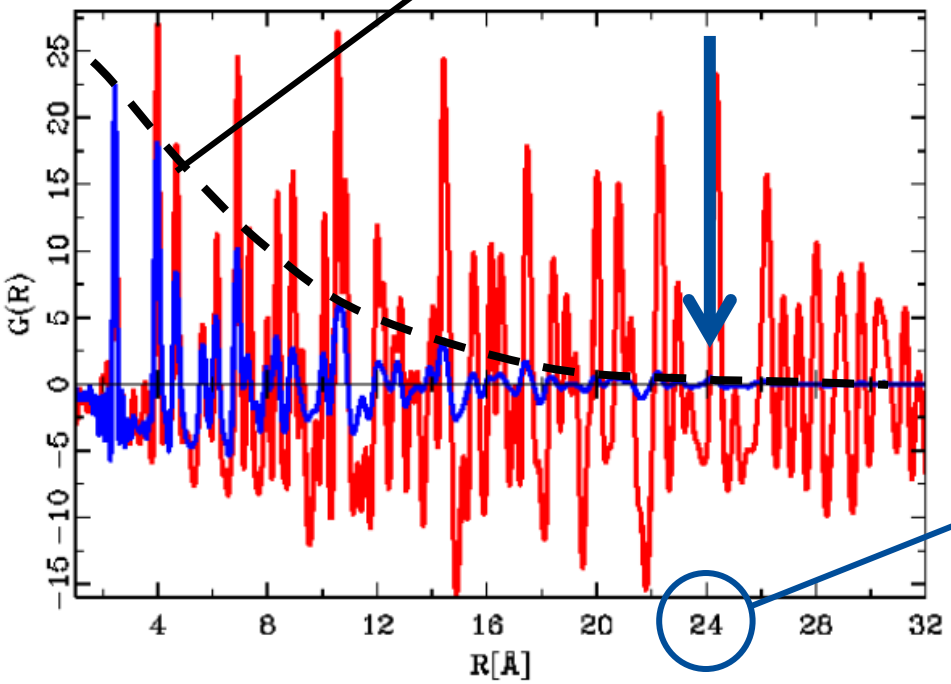

crystalline ZnSe

nanocrystaline ZnSe

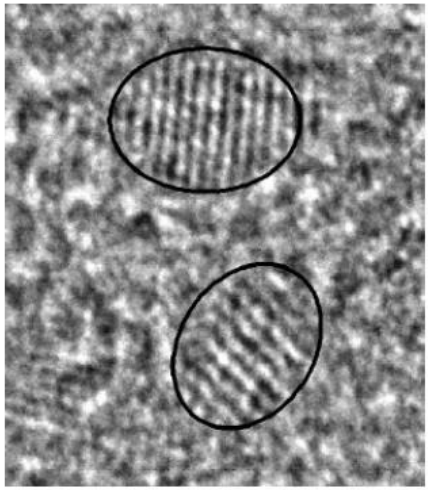

→ Courtesy of R. Neder

PDF OF NANOPARTICLE SYSTEMS

Indication of stacking faults

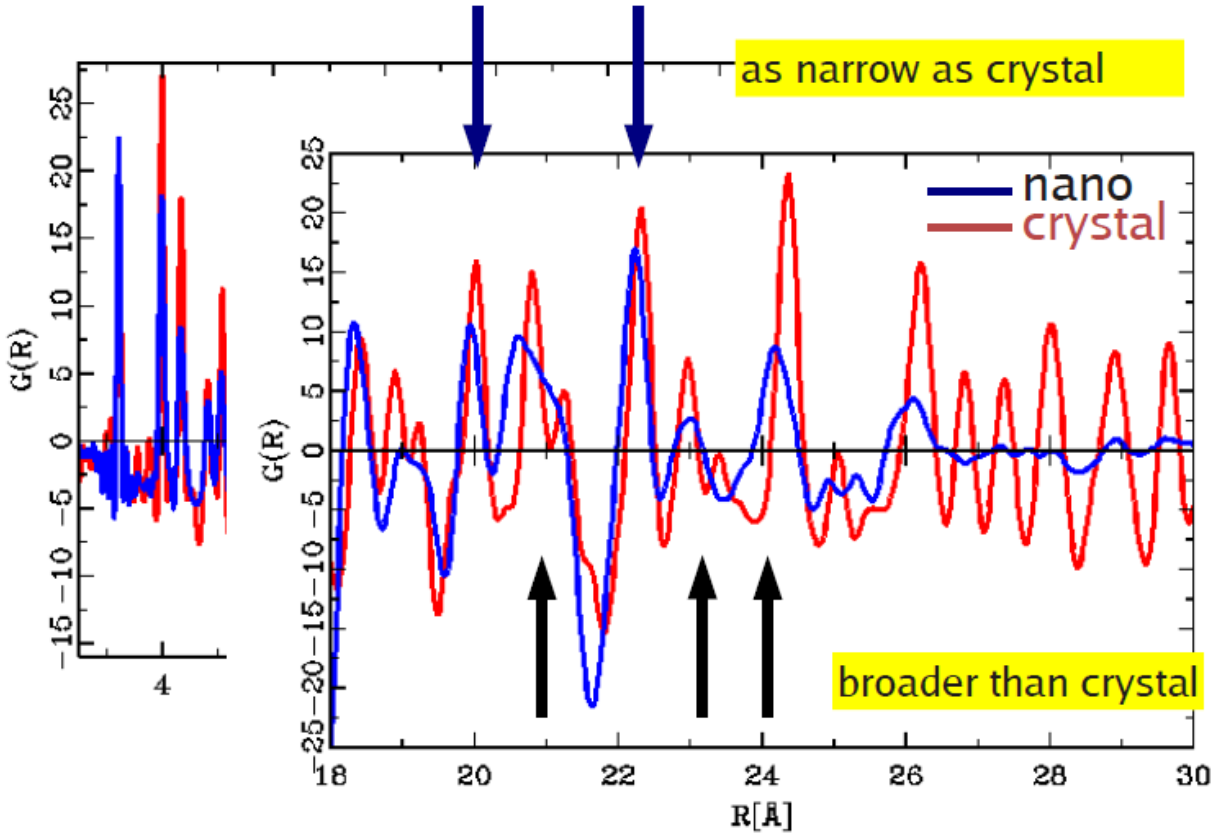

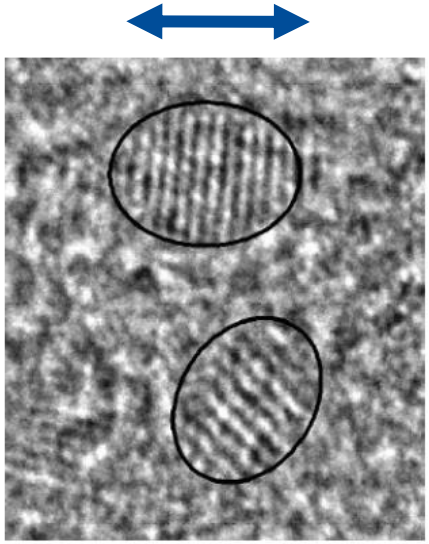

→ Courtesy of R. Neder

PDF ANALYSIS OF NANOPARTICLE SYSTEMS

Au nanoparticle + ligand

Au + S-CH2-CH2-(CF2)5-CF3

Gold -Ligand
Au – S 2.42Å

Ligand -
Ligand
C-C 1.5Å
C-F 1.3Å

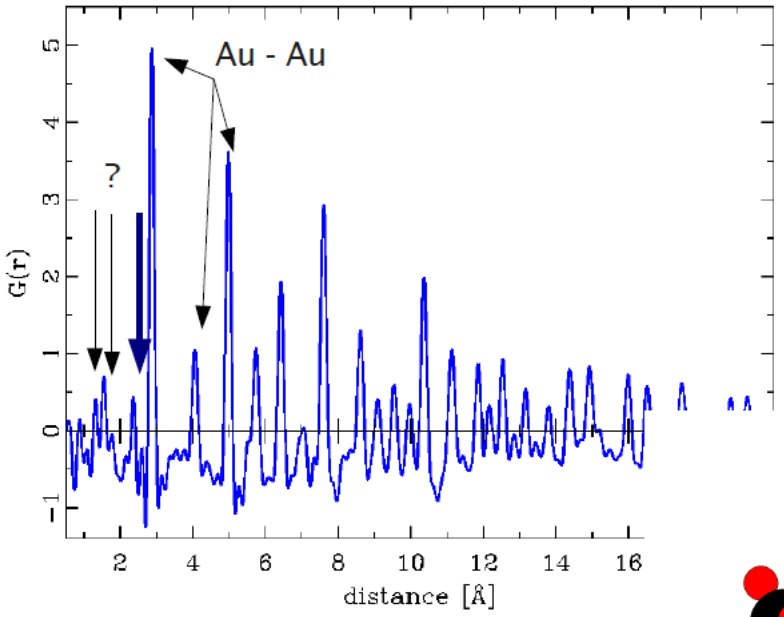

Au
F m 3 m
a 4.064 Å
Au-Au 2.837Å

Number ?
Placement ?
Composition ?

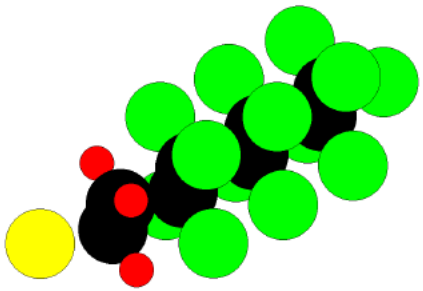

15 K
NPDF, Los Alamos
Page, *et al.*, *Chem. Phys. Lett.* **393** (2004) 385-388.

→ Courtesy of R. Neder

PDF ANALYSIS OF NANOPARTICLE SYSTEMS

Au nanoparticle + ligand

Au + S-CH2-CH2-(CF2)5-CF3

Gold -Ligand
Au – S 2.42Å

Ligand - Ligand
C-C 1.5Å
C-F 1.3Å

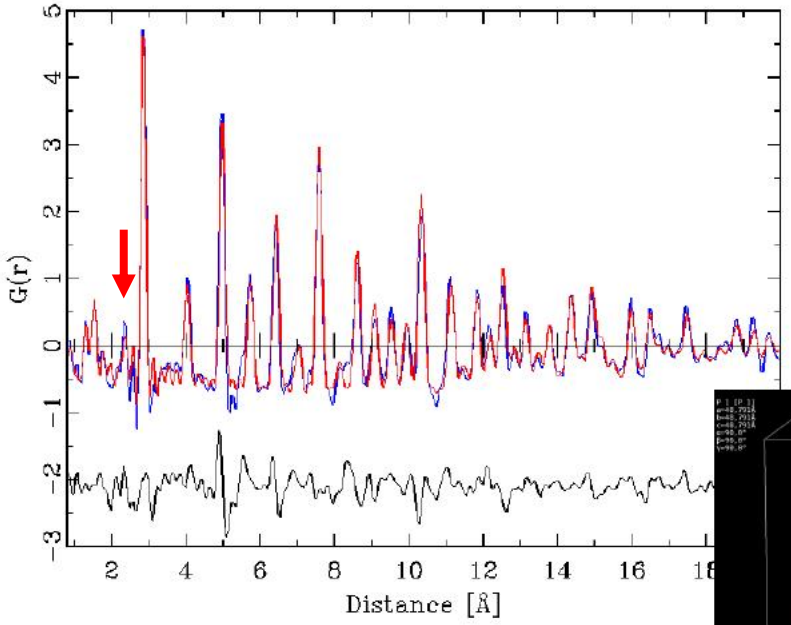

15 K
NPDF, Los Alamos
K. Page et al. J. Appl. Cryst. (2011)

a(Au)	4.0658Å	(1)
Au – Au	2.8750Å	(1)
B(Au)	0.32Å^2	(4)
B(Ligand)	0.45Å^2	(10)
Diameter	20Å	(2)
N(ligand)	20	(6)
P(Fluorine)	0.65	(15)
Au – S	2.42Å	fixed!

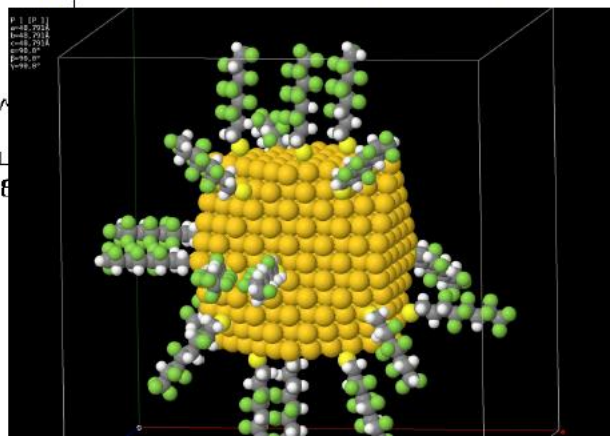

Bottom-up modelling DISCUS DIFFEV

→ Courtesy of R. Neder

TOTAL SCATTERING TECHNIQUES

PDF approach

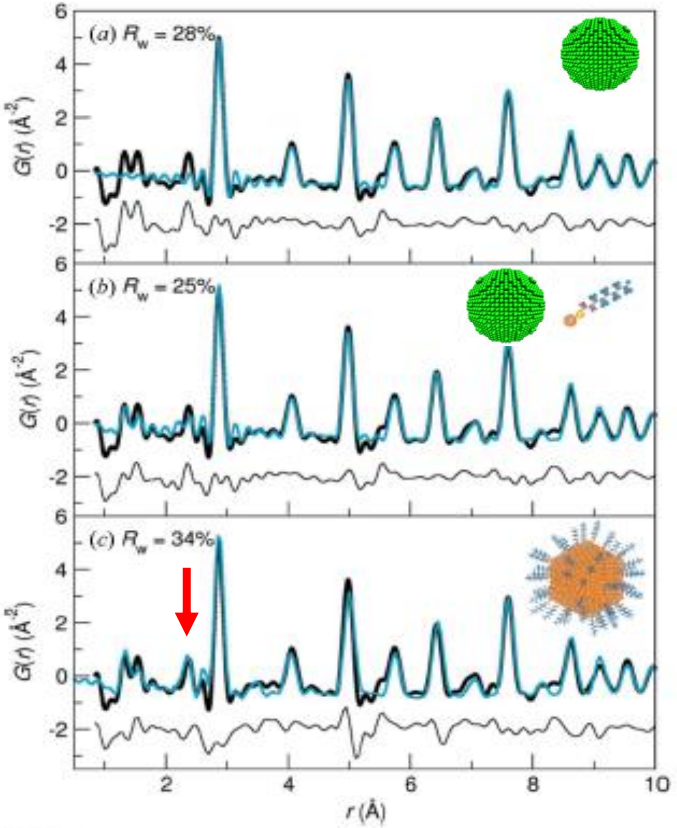

Figure 5
The first 10 Å of three 20 Å fits to 15 K data from Au nanoparticles. Data are shown as circles and fits as lines through the data, and difference curves lie below. (*a*) Fit from single-phase (f.c.c. Au) refinement using *PDFgui*. (*b*) Fit from two-phase refinement using *PDFgui*. (*c*) Fit from finite ligand-capped nanoparticle model using *DIFFEV*.

K. Page et al., J.Appl.Cryst. 44 (2011) 327

Debye Scattering Equation

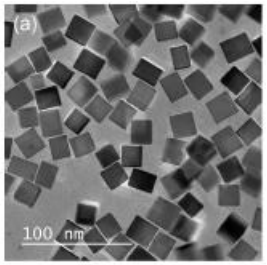

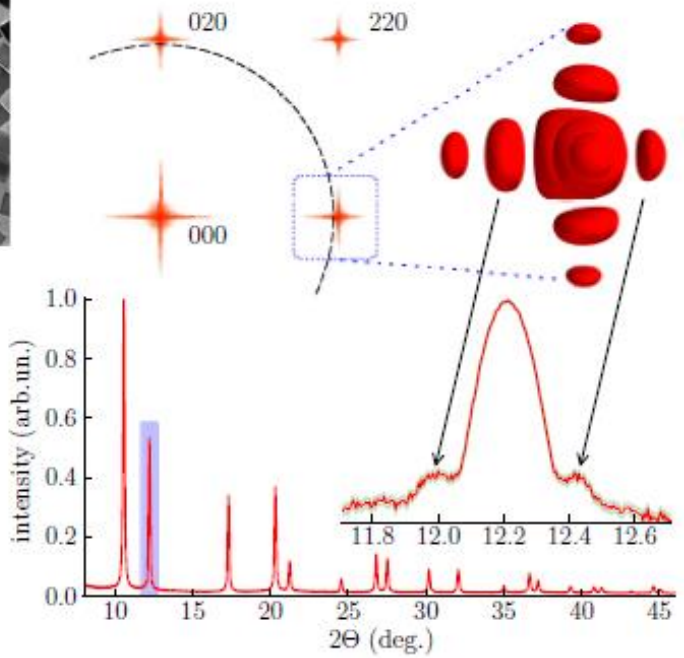

FIG. 2. (Color online) Experimental x-ray powder pattern for the studied Pd nanocrystals. The inset shows a detail of the (200) peak. Arrows on the latter indicate the interference fringes from the parallel 100 facets of the nanocrystals, which correspond to the analogous features observed in reciprocal space (RS) (above): Powder diffraction integrates information over spheres of growing radius in RS, as schematically represented in the inset of the upper figure.

P. Scardi et al., Phys. Rev. B91 (2015) 155414

TOTAL SCATTERING TECHNIQUES

PDF approach

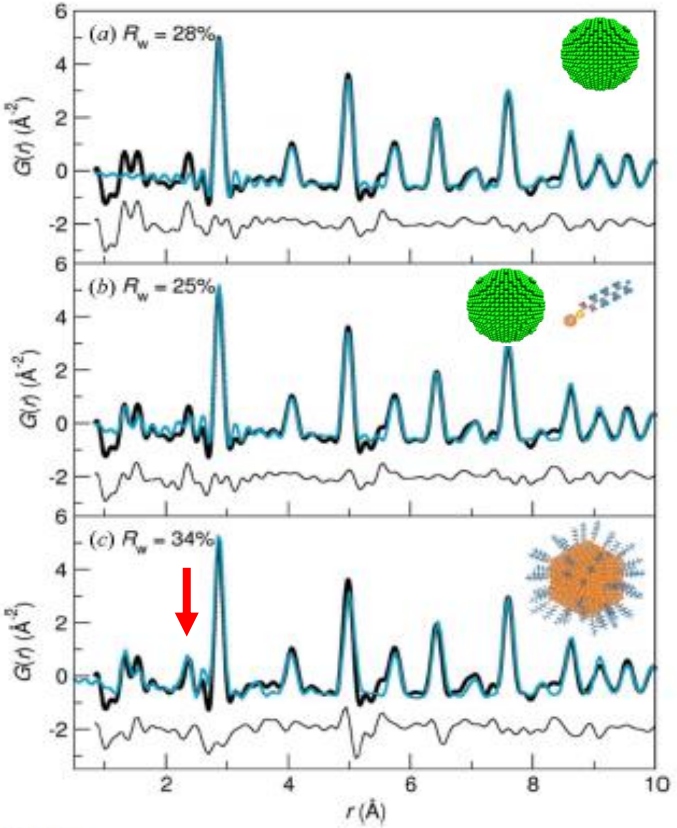

Figure 5
The first 10 Å of three 20 Å fits to 15 K data from Au nanoparticles. Data are shown as circles and fits as lines through the data, and difference curves lie below. (*a*) Fit from single-phase (f.c.c. Au) refinement using *PDFgui*. (*b*) Fit from two-phase refinement using *PDFgui*. (*c*) Fit from finite ligand-capped nanoparticle model using *DIFFEV*.

K. Page et al., J.Appl.Cryst. 44 (2011) 327

Debye Scattering Equation

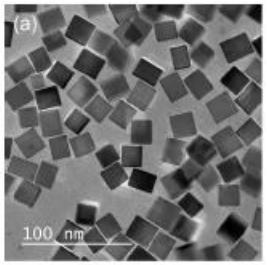

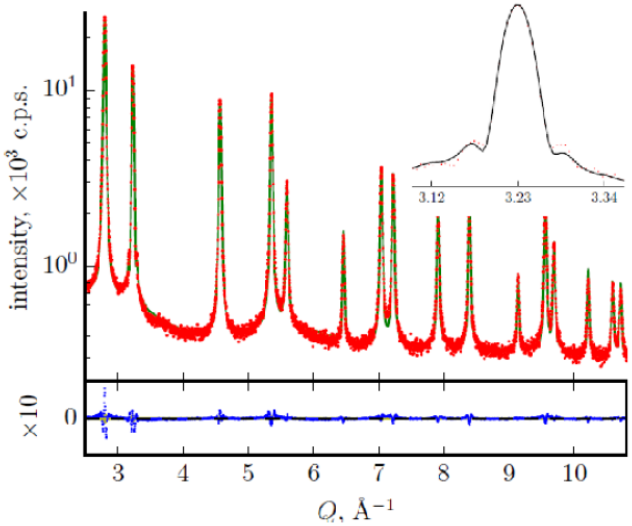

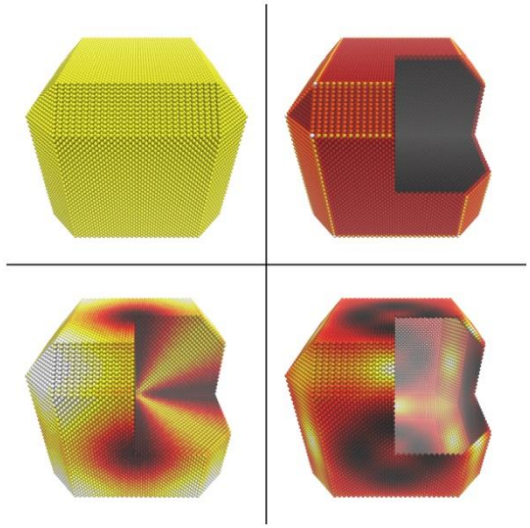

P. Scardi & L. Gelisio, DSE2015

DIFFRACTION FROM NANOCRYSTALLINE MATERIALS

1. Traditional reciprocal space approach : sum & average

$$I_{PD}(s) \propto \frac{\int I_{sc}(\underline{s})\,d\Omega}{4\pi s^2} = |F|^2 \left\{ I^{IP}(s) \otimes I^{S}(s) \otimes I^{D}(s) \otimes I^{F}(s) \otimes I^{APB}(s) \otimes I^{C}(s) \otimes I^{GRS}(s) \ldots \right\}$$

2. Total Scattering methods

Direct (real) space approach: average & sum
Debye Scattering Equation (DSE)

$$I_{PD}(s) = |f|^2 \sum_m \sum_n \frac{\sin(2\pi s r_{mn})}{2\pi s r_{mn}}$$

Pair Distribution Function (PDF)

$$g(r) = \frac{\rho(r)}{\rho_0} = 1 + \frac{1}{2\pi^2 \rho_0 r} \int_0^\infty Q\left[S(Q) - 1\right] Sin(Qr)\,dQ$$

$$I(s) = N|f|^2 \left\{ 1 + \frac{1}{2\pi s} \int_V 4\pi r \left[\rho(r) - \rho_0\right] Sin(2\pi s r)\,dr \right\}$$

DIFFRACTION FROM NANOCRYSTALLINE MATERIALS

Current research / future trends

→ toward an integration between atomistic modelling and diffraction analysis: real structure of nanoparticle systems

Debye Scattering Equation

$$I_{PD}(s) = |f|^2 \sum_m \sum_n \frac{\sin(2\pi s r_{mn})}{2\pi s r_{mn}}$$

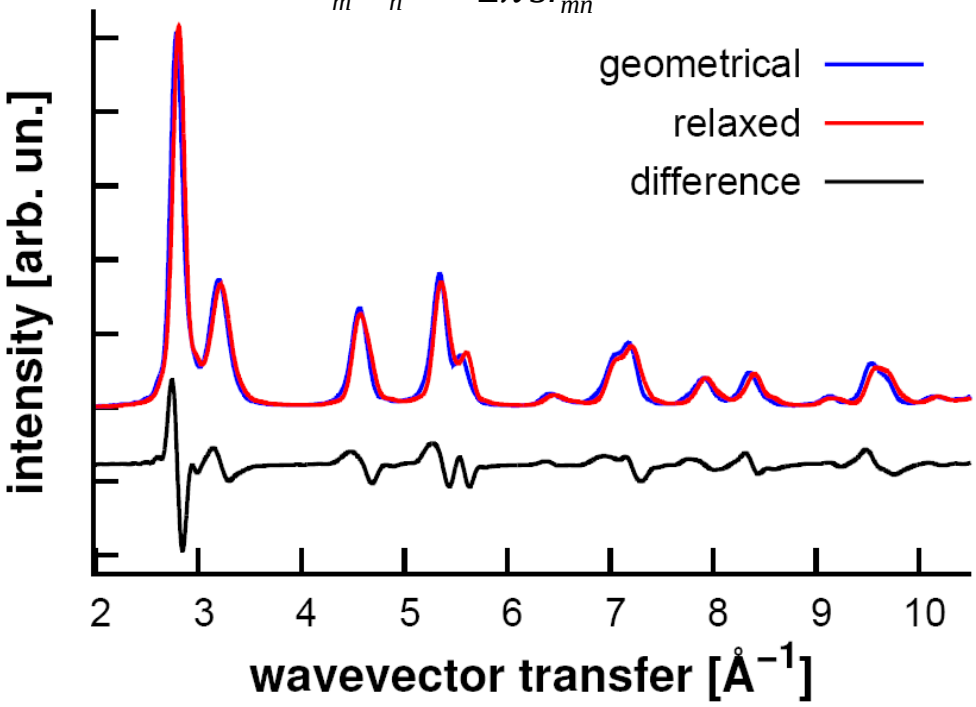

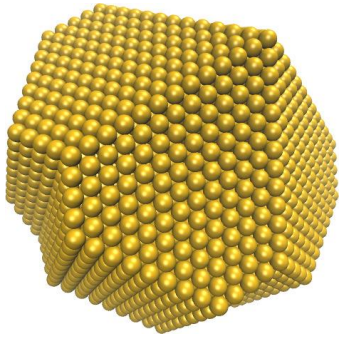

geometrical

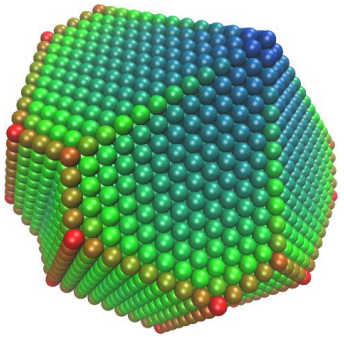

relaxed
(energy minimization)

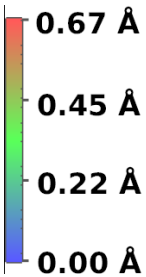

Scardi & Gelisio, Sci. Reports 6 (2016) 22221

DIFFRACTION FROM NANOCRYSTALLINE MATERIALS

Current research / future trends

→ toward an integration between atomistic modelling and diffraction analysis: plastically deformed nanocrystalline systems; grain boundary, line and planar defects

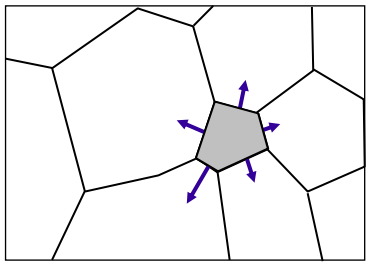

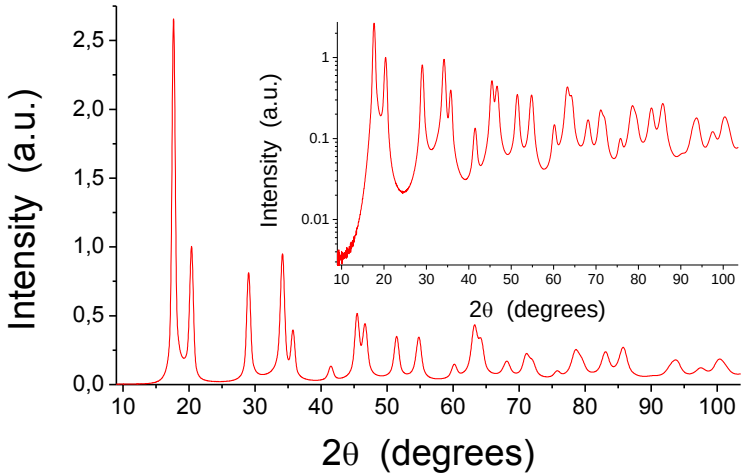

P. Scardi et al. J. Appl. Cryst. 50 (2017) 508

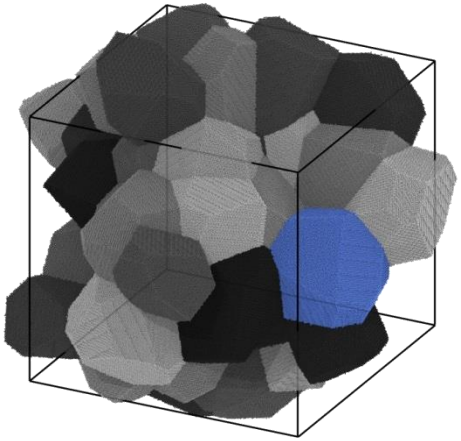

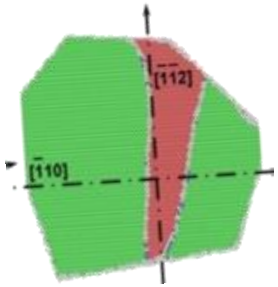

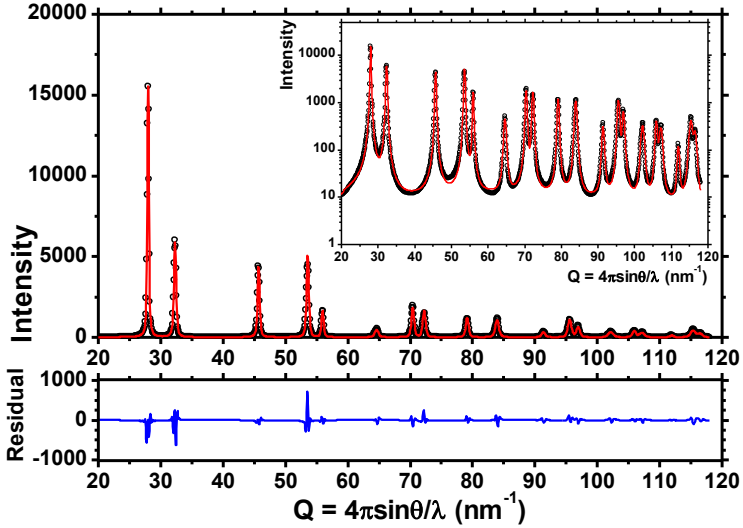

A. Leonardi & P. Scardi, Met. Mat.Trans A 47 (2016) 5722

GENERAL REFERENCES

B.E. Warren, *X-ray Diffraction*, Addison-Wesley, Reading, MA, 1969.

A. Guinier, *X-ray Diffraction*, Freeman & Co, S. Francisco, 1963.

A.J.C. Wilson, *X-ray Optics*, 2nd ed., Methuen & Co, London, 1962.

H.P. Klug & L.E. Alexander, *X-ray Diffraction procedures*, Wiley, New York, 1974.

B.D. Cullity, *Elements of X-ray Diffraction*, Addison-Wesley, Reading Ma, 1978.

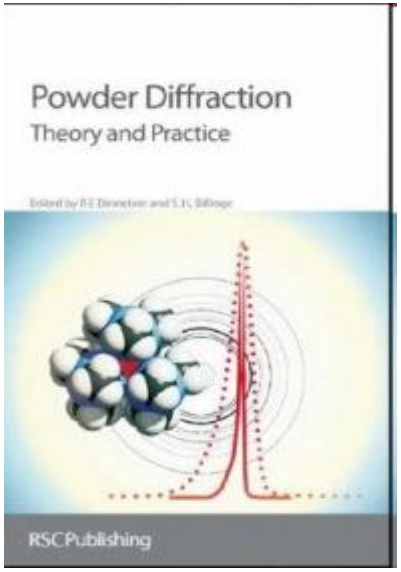

Powder Diffraction: Theory and Practice
R.E. Dinnebier & S.J.L. Billinge, editors.
Cambridge: Royal Society of Chemistry, 2008.

P. Scardi, Chapter 13 on Line Profile Analysis:

REFERENCES - Paolo.Scardi@unitn.it

Extending the Reach of Powder Diffraction Modelling by User Defined Macros
P. Scardi & R. E. Dinnebier, editors
A special issue of Materials Science Forum, 2010.

Diffraction Analysis of Materials Microstructure
E.J. Mittemeijer & P. Scardi, editors.
Berlin: Springer-Verlag, 2004.

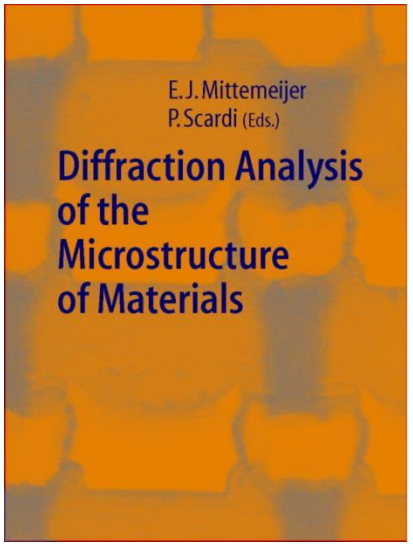

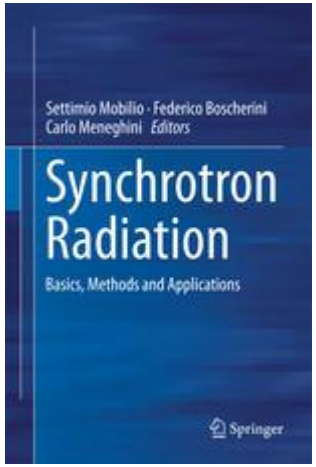

Synchrotron Radiation. Basics, Methods and Applications
S. Mobilio, F. Boscherini, C. Meneghini, editors.
Springer-Verlag, 2015